Progress in Polymer Science 70 (2017) 34–51

Contents lists available at ScienceDirect

Progress in Polymer Science

journal homepage: www.elsevier.com/locate/ppolysci

Review

Recent advances in high performance donor-acceptor polymers for organic photovoltaics

Sarah Holliday[a], Yilin Li[a], Christine K. Luscombe[a,b,*]

[a] Materials Science and Engineering Department, University of Washington, Seattle, WA 98195-2120, USA
[b] Department of Chemistry, University of Washington, Seattle, WA 98195-1700, USA

ARTICLE INFO

Article history:
Received 29 September 2016
Received in revised form 10 March 2017
Accepted 10 March 2017
Available online 22 March 2017

Keywords:
Organic photovoltaic
Conjugated polymer
Semiconducting polymer
Bulk heterojunction
Solar cell

ABSTRACT

Organic photovoltaic cells made with semiconducting polymers remain one of the most promising technologies for low-cost solar energy due to their compatibility with roll-to-roll printing techniques. The development of new light-absorbing polymers has driven tremendous advances in the power conversion efficiency of these devices. In particular, the use of alternating electron rich (donor) and electron poor (acceptor) segments along the polymer backbone can produce low optical bandgap materials that capture more of the solar spectrum. As a result, power conversion efficiencies over 10% are increasingly common for this technology. This review summarizes the recent advances in donor-acceptor polymer design and synthesis, highlighting the structural features that are key to providing high efficiency, scalable and stable devices.

Contents

* Corresponding author at: Materials Science and Engineering Department, University of Washington, Seattle, WA 98195-2120, USA.
E-mail address: luscombe@uw.edu (C.K. Luscombe).

http://dx.doi.org/10.1016/j.progpolymsci.2017.03.003
0079-6700/

1. Introduction

Organic photovoltaics (OPVs), which utilize light absorbing polymers or small molecules to generate an electrical current from light, have received significant attention in recent years as a form of highly scalable and inexpensive solar energy production. In contrast to the relatively heavy and brittle modules made with inorganic semiconductors such as silicon, OPVs offer the attractive prospect of low-temperature, solution processed fabrication such as roll-to-roll and inkjet printing, that have the potential to dramatically lower the cost of solar energy production. Furthermore, the potential for large-area, lightweight and mechanically flexible modules, with options for semi-transparent and colored films, opens up new opportunities for building-integrated photovoltaics among other applications [1–3]. The field of OPV has advanced enormously in the last few decades, with frequent reports now of lab-scale efficiencies >10%, which is often stated as the benchmark for commercial viability [4]. A large part of this progress can be attributed to the development of new light-absorbing polymers. From the simple homopolymers such as MDMO-PPV and P3HT that were popular in the early days of the field [5–7], hundreds of more complex polymer structures have since been introduced with improved light absorption, charge generation and charge transport properties [8–10]. Significant advances have also been made in other integral components of the device including the electron acceptor [11,12], electrodes and interfacial layers [13,14]. In this review, we will detail the recent advances made in donor-acceptor (D-A) copolymers for OPV applications, with particular focus on key polymer structural features that contribute to their high performance. As a rough benchmark for high performance, we have included only polymers demonstrating power conversion efficiencies of 8% or over in this review.

2. Working principles of OPV

2.1. Bulk heterojunction OPV

Organic materials, which are typically considered insulators, can become semiconductors when they possess sufficient conjugated π-bonding character. As the number of alternating single and double bonds in a π-bonded system is increased, such as in a highly conjugated (sp^2 hybridized) polymer or small molecule, the overlap of atomic orbitals increases and thus the energy gap between the highest occupied molecular orbital (HOMO) and the lowest unoccupied molecular orbital (LUMO) becomes smaller. When this energy gap becomes small enough, the absorption of visible light can photo-excite an electron in the material across this gap, analogous to the band model of inorganic semiconductors. However, in contrast to inorganic semiconductors, in which free electron-hole pairs are produced upon photoexcitation, the photoexcitation of organic semiconductors produces bound electron-hole pairs, also known as excitons. These excitons have a large binding energy (typically 0.2–1.0 eV) that drives the electron and hole to recombine after photoexcitation [15]. A solution to this problem was proposed by Tang et al. in 1986 [16], which involves combining two organic semiconductors with slightly offset HOMO and LUMO energies, such that the photoexcited electron in the first material (the 'donor') is transferred to the second material ('acceptor'), allowing for the charges to be separated at the junction between these two materials.

Fig. 1 demonstrates a simplified energy diagram for the process of charge separation at this heterojunction. When the donor absorbs a photon, an electron is initially excited across the bandgap from the HOMO to the LUMO, forming an exciton (i). This exciton then diffuses towards the donor-acceptor interface, where the

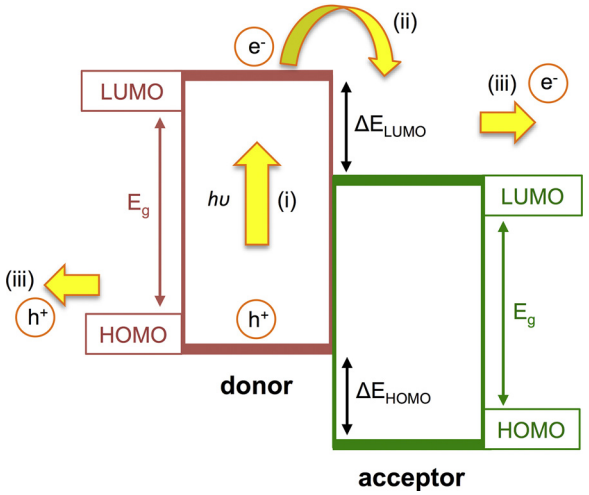

Fig. 1. Simplified energy level diagram for a donor-acceptor heterojunction in an OPV device with basic charge generation and separation processes indicated as follows: (i) absorption of a photon with energy $>E_g$, causing an electron to be excited in the donor to form an exciton; (ii) transfer of the electron to the acceptor; (iii) drift of electron and hole towards the electrodes.

electron can be transferred to the LUMO of the acceptor material, provided that the difference between the LUMO energies (ΔE_{LUMO}) of the donor and acceptor is greater than the exciton binding energy (ii). Likewise, for an exciton that is formed on the acceptor, hole transfer to the donor can occur if the energy offset between the HOMO energies (ΔE_{HOMO}) is sufficient. It is from this weakly bound charge transfer (CT) state that the free electron and hole can be generated, which can then drift towards their respective electrodes (iii). However, it is also possible that the exciton can recombine at the heterojunction prior to becoming free charges (geminate recombination), or alternatively recombine with other free charges generated from separate absorption events (non-geminate recombination), and both of these processes can result in significant efficiency losses in OPV devices [17].

The very short diffusion length of excitons (average length an exciton moves between generation and recombination) in most organic semiconductors (around 10 nm) adds a further challenge, as the donor and acceptor phases must to be close enough for excitons to reach the interface in order to separate. For this reason, the donor and acceptor components are typically blended on the nanoscale to form a bulk heterojunction (BHJ). This morphological strategy was first proposed in the early 1990s [18,19], and has since remained the prevalent active layer structure in OPV research. Compared to a bilayer structure, the BHJ archetype allows relatively thick films of the active layer blend to be deposited so that more light can be absorbed, while maintaining a large number of donor-acceptor interfaces for efficient exciton dissociation. Such BHJ films are typically fabricated by co-depositing the two semiconductors from a mixed solution, and allowing the two materials to phase separate upon drying to form nanoscale domains of donor and acceptor. In practice, predicting and controlling the extent of this phase separation is extremely challenging, as will be discussed in Section 2.5.

2.2. Solar cell characterization

The photovoltaic performance of a solar cell can be characterized by illuminating the cell and obtaining the current density (J, output current divided by the device illuminated area) in response to an applied voltage (V). Several important parameters can be extracted from this J-V curve, including the current density at short circuit (J_{SC}), the voltage at open circuit (V_{OC}) and the fill factor (FF). The

FF is defined as the product of current density and voltage at the point of maximum power density (J_{MP}, V_{MP}) divided by the product of the J_{SC} and V_{OC}, as outlined in Eq. (1):

$$FF = (J_{MP} \times V_{MP})/(J_{SC} \times V_{OC}) \quad (1)$$

The power conversion efficiency (PCE) of a solar cell is the ratio of how much power the cell can generate relative to the incident power from the sun. As outlined in Eq. (2), this can be calculated from the product of the J_{SC}, V_{OC} and FF divided by the incident power density P_i, which is typically standardized as 100 mW cm^{-2} using a solar simulator set to AM1.5G:

$$PCE = (J_{SC} \times V_{OC} \times FF)/P_i \quad (2)$$

All of the performance metrics listed above can be affected by multiple different factors. The J_{SC} will depend on the amount of light absorbed, as well as the efficiency of charge generation and losses associated with charge recombination, charge carrier mobility and the efficiency of charge collection at the electrodes. The V_{OC} is a measure of the maximum electrochemical potential of the cell and can be approximately related to the energy offset between the HOMO of the donor and the LUMO of the acceptor. This is susceptible to various loss mechanisms which limit the device efficiency, an aspect that has received increasing attention in recent years [20]. As will be demonstrated throughout this review, one of the biggest challenges in OPV has been in balancing the need for a low bandgap in the donor polymer (to maximize J_{SC}) with the need for a low-lying HOMO in the donor (to maximize V_{OC}). The FF, meanwhile, is influenced by factors that determine how easily charges can be extracted from the device. These include the relative charge carrier mobilities of the donor and acceptor as well as the active layer morphology and various interfacial effects that can affect the charge collection [21].

2.3. Device architectures

In order to make a photovoltaic cell, the semiconducting active layer is sandwiched between two electrodes. In the conventional cell architecture, a high work function, transparent and conducting anode such as indium tin oxide (ITO) is typically used, with a hole selective interlayer such as poly(ethylenedioxythiophene):poly(styrene sulfonic acid) (PEDOT:PSS) between the anode and the active layer to facilitate hole injection. A low work function metal such as Al is then used as the cathode, often with an additional thin layer of Ca or LiF to create a favourable surface dipole at the interface for better electron injection. While this conventional architecture remains widely used, it suffers from stability issues due to the oxidation of low work function metals such as Ca and Al, as well as the presence of pinholes that can allow oxygen and water to react with the active layer [22]. In addition, the highly acidic nature of PEDOT:PSS can lead to further device degradation by reacting with the active layer or via etching of the ITO [23]. An alternative to the conventional architecture is an inverted one, wherein an n-type semiconductor (e.g. ZnO or TiO_x) is layered on the ITO to facilitate electron collection, which allows a high work function, and therefore relatively air stable, metal such as Ag to be used as the top electrode. MoO_3 or other transition metal oxides are often deposited in this case as the hole selective interlayer, in place of PEDOT:PSS. As well as demonstrating significantly improved stability, inverted devices can in many cases lead to higher efficiencies which has contributed to the increasing popularity of this architecture in recent years [24,25].

2.4. Electron acceptor materials

BHJ devices require an electron acceptor alongside the light-absorbing polymer donor. From the early days of OPV research, the materials used for this have been almost universally a fullerene derivative, such as the archetypal phenyl-C_{61}-butyric acid-methyl ester ($PC_{61}BM$) [26]. One of the main problems with fullerene-based acceptors is their high degree of molecular symmetry, which leads to extremely limited absorption in the visible and near-IR spectral regions. Given that the acceptor is accountable for approximately half of the volume of the active layer, it significantly limits the available photocurrent if this material does not absorb visible light. The reduced symmetry of the C_{70} analogue phenyl-C_{71}-butyric acid-methyl ester ($PC_{71}BM$) results in more allowed optical transitions and therefore significantly stronger absorption in the visible region, which accounts for the widespread popularity of this fullerene in high performance devices. However, the cost of $PC_{71}BM$ production is even higher (market price ~$900/g) than for $PC_{61}BM$ (~$300/g), creating a significant barrier to commercial scale-up. Another critical issue with fullerene acceptors is their strong tendency to diffuse through the polymer and self-aggregate over time, a process that is particularly accelerated by heat [27,28]. Furthermore, the optoelectronic properties of these acceptors are not easily modified, since the addition of substituents to the fullerene cage (e.g. via cycloaddition reactions) does not allow for direct conjugation and therefore the only ways of modifying the energy levels are via weaker inductive effects [29,30]. In particular, the large electron affinity of most fullerenes makes them very effective electron acceptors, but the ability to decrease it slightly would be of significant benefit for the V_{OC}. The difficulty in achieving this with fullerenes is one reason why chemists have instead focussed on developing donor polymers with large ionization potentials to increase the V_{OC}. It should be noted that some fullerenes with smaller electron affinities do exist that give a higher V_{OC}, the most successful of which is indene-C_{60}-bisadduct (ICBA), but its cost is also prohibitively high (~$1700/g).

Considering these shortcomings, it is not surprising that many attempts have been made to develop alternative, non-fullerene acceptors. One strategy is to use n-type polymers, but progress here has been limited somewhat by difficulties in obtaining a well-dispersed morphology in polymer-polymer blends [31]. An alternative approach is to employ electron deficient, conjugated small molecules. Tremendous advances have been made in this area within the past few years, with the design of new small molecule acceptors that can now match or even outperform fullerenes [11,12,32]. Indeed, some of the highest device efficiencies to date are achieved with non-fullerene acceptors [33]. One advantage of using small molecule acceptors is that, unlike fullerenes, the HOMO and LUMO levels can be easily tuned by changing the chemical structure, allowing the energetic offset between donor and acceptor to be more readily optimized. This is exemplified by multiple reports of fullerene-free devices giving V_{OC} values greater than 1 V [34–38], a difficult value to match with fullerene acceptors [39,40]. It also allows for the bandgap of the acceptor to be tuned, making absorption at longer wavelengths a possibility. This provides an exciting avenue for OPV research since the donor polymer no longer needs to be considered as the main absorber at long wavelengths, as has traditionally been the case with fullerenes. In addition, the crystal packing properties of small molecules can be easily tuned by the choice of various solubilizing alkyl chains, in order to control the active layer morphology. With the growing library of small molecule acceptors that is now materializing, the future of OPV research will increasingly involve carefully selecting both donor and acceptor to achieve the best match in terms of energy levels, spectral coverage and morphology [41,42].

2.5. Active layer morphology

The microstructure of the active layer BHJ in an OPV device plays a key part in determining the performance, but is also one of the aspects that is most difficult to control [43–46]. The aim is to achieve a bicontinuous network of donor and acceptor domains between 10 and 20 nm, providing a large interfacial area between the two domains to allow for exciton dissociation, while forming a continuous percolating pathway to transport free charges to the electrodes. The degree of phase separation is critical, since domains that are too large (greater that the exciton diffusion length) will favor geminate recombination [47,48], whereas too little phase separation can increase the rate of non-geminate recombination [28]. Further complexity arises from the fact that there can be significant miscibility between the polymer and fullerene in some blends [49]. This led to the development of a three phase model, whereby a mixed, amorphous region exists alongside discrete polymer and fullerene domains [49–51]. Analytical tools such as resonant soft X-ray scattering (R-SoXS)[52–54], scanning transmission X-ray microscopy (STXM) [52,55], near-edge X-ray absorption fine structure (NEXAFS) spectroscopy[50] and spectroscopic ellipsometry[56] have helped refine this picture further to allow for the quantitative evaluation of domain purity. However, the exact influence of domain purity on solar cell performance is still under debate. It has been shown that the energetic cascade formed between ordered and disordered (mixed) regions can create a driving force for charge separation at this interface, helping to sweep charges out of the disordered region towards the electrodes [57,58], suggesting that at least some degree of miscibility is beneficial. Conversely, there is evidence that impure domains lead to an increase in recombination losses and low charge carrier mobility, and this is found to be particularly limiting in the case of thicker films [59,60]. Some of the highest performing polymer blends employing relatively amorphous benzodithiophene-based polymers such as PTB7 (Section 3.1) have been suggested to have hierarchical morphologies [54,61] or even no pure polymer domains at all [52]. On the other hand, many of the recent crystalline oligothiophene-based donor polymers (Section 4) exhibit small but extremely phase-pure domains, and demonstrate equally high efficiencies [62]. On this basis it has been proposed that a single, 'ideal' morphology may not actually exist, but rather multiple different morphologies that can all lead to high efficiency devices [63,64]. The active layer is typically prepared by co-depositing the donor and acceptor from solution, and allowing these two materials to phase separate upon drying. In a laboratory setting, spin-coating is most widely used for this since it is a relatively easy, versatile and inexpensive method of depositing thin films for test scale devices [65,66]. Multiple factors can affect the drying kinetics of the film, including the choice of casting solvent (boiling point, viscosity, polarity, surface tension etc), solute concentration, temperature (of both substrate and casting solution), deposition rate and annealing steps (thermal or solvent vapour annealing), and typically these parameters must all be optimized by a somewhat trial-and-error approach to optimize the morphology for a particular blend. Unfortunately, this technique is rather wasteful of material since the majority of solution that is dispensed onto the substrate is ejected during spin-coating, and it is also inherently unsuitable for depositing large areas (over a few cm^2). Techniques such as slot-die coating or inkjet printing are considerably more scalable, but care must be taken in transferring to more scalable methods since the resulting morphology can vary dramatically [63,67]. High-boiling solvents such as chlorobenzene and dichlorobenzene are normally used to deposit the film in order to allow the materials sufficient time to self-organize and phase separate as the film dries. In addition, an even higher boiling solvent such as chloronaphthalene (CN) or 1,8-diiodooctane (DIO) is often added in small amounts (1–5 vol%). These solvent additives can improve the film morphology by selectively dissolving one of the active layer components, and by allowing this component to remain in solution for longer during film formation because of the significantly higher boiling point of the additive relative to the host solvent [68]. DIO has been especially useful in blends containing $PC_{71}BM$ as it has been shown to effectively prevent the formation of large $PC_{71}BM$ aggregates that can be detrimental to device performance. Due to the greater solubility of $PC_{71}BM$ in DIO relative to the polymer, it remains in solution during film formation, allowing it sufficient time to penetrate the polymer network during film drying, as demonstrated in Fig. 2 [52,61,69–71]. The more finely dispersed morphology can be beneficial for charge generation, reducing recombination (both geminate and non-geminate) and increasing charge carrier mobility in the blend [72]. It has also been suggested that DIO results in a more favourable concentration gradient within the active layer to further improve charge pair dissociation and reduce recombination [61]. As such, the majority of high performance OPV devices that are published now use solvent additives. However, the added complexity for device fabrication, as well as the toxicity of DIO, creates a disadvantage for large-scale manufacture. There is also evidence that some additives can be detrimental for device stability. The high boiling point of DIO (332.5 °C at 760 mmHg) means that it is difficult to remove from the film after device fabrication, with some reports suggesting that a small amount remains even after electrode deposition [73]. DIO is also unstable to light [74], forming radical species that may cause degradation of the polymer if not fully removed [75].

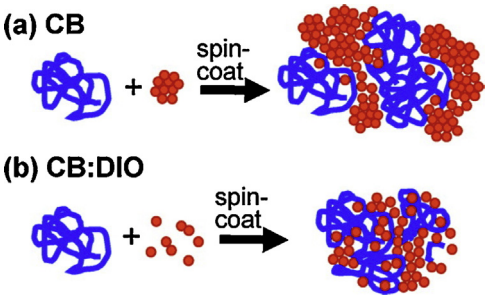

Fig. 2. Schematic of proposed PTB7 (blue) and $PC_{71}BM$ (red) aggregation in (a) chlorobenzene (CB) and (b) chlorobenzene with DIO additive. [71], Copyright 2011, Reprinted with permission from the American Chemical Society. (For interpretation of the references to colour in this figure legend, the reader is referred to the web version of this article.)

2.6. Donor-acceptor polymers

Since most fullerene acceptors do not absorb strongly in the visible and near-IR portion of the spectrum, where solar radiation is highest, the role of light absorption in OPV devices has traditionally fallen on the donor. This means that a large amount of the research has focused on reducing the optical bandgap E_g of the polymer. As described in Section 2.1, the bandgap in semiconducting polymers arises from overlap of π-orbitals, and therefore can be reduced by creating a more planar polymer backbone in order to extend the conjugation. Various techniques have been employed by chemists to this end, such as using fused ring systems (e.g. thienothiophene, benzodithiophene) and bridging atoms (e.g. fluorene, indenofluorene, cyclopentadithiophene), as well as increasing the degree of quinoidal character and minimizing torsion due to steric effects along the backbone. For example, the increased quinoidal character of the two thiophene rings in Fig. 3a leads to greater sp^2 bonding character compared to the two coupled phenyl units, and this therefore favors a more planar conformation. A further planarization effect occurs in this case due to the

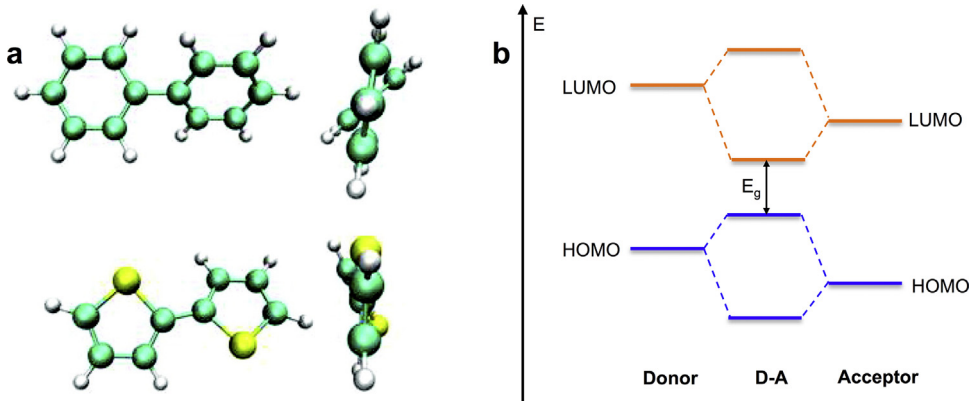

Fig. 3. (a) Comparison of the torsional angle between two coupled phenyl (top) and thienyl (bottom) rings; [79], Copyright 2012, Adapted with permission from the American Chemical Society; (b) Diagram showing reduced bandgap E_g in donor-acceptor (D-A) polymers via molecular orbital hybridization.

reduced steric torsion effects from the α–protons on coupled thiophene rings compared to those on adjacent phenyl groups. For this reason, thiophene based polymers have been ubiquitous in the field of organic electronics for some time, most notably in the form of poly(3-hexylthiophene) (P3HT), which remains one of the most widely used polymers in OPV research [7,76]. The planar backbone of P3HT is also beneficial for charge carrier mobility due to the shorter intermolecular contacts between chains, resulting in hole mobilities of 0.1–0.3 $cm^2 V^{-1} s^{-1}$ for this polymer in organic field effect transistors [77,78].

Despite its very planar backbone, P3HT has a relatively wide bandgap of around 1.9 eV, which means that this polymer can only harvest approximately 22% of photons from the sun and this limits the J_{SC} that can be generated [80]. In order to further reduce the bandgap, the technique of donor-acceptor (D-A) hybridization is now widely used, whereby alternating electron-rich and electron-poor segments are incorporated along the polymer backbone. The molecular orbital mixing that occurs between of the conjugated donor (D) and acceptor (A) units leads to the formation of a new set of hybridized molecular orbitals with an effective bandgap E_g that is smaller than either of the individual components, as demonstrated in Fig. 3b. This allows D-A polymers to achieve significantly lower bandgaps than via backbone planarization alone, which can account for their rise in popularity in OPV research [8,10,81]. Control over the bandgap and the energy levels can be achieved by judicious choice of monomers, since the HOMO and LUMO of the polymer are principally determined by the HOMO and LUMO of the donor and acceptor components, respectively. Popular electron-rich donor units include fused and bridged thiophene-based ring systems such as benzodithiophene (BDT), indacenodithiophene (IDT) and cyclopentadithiophene (CPDT), for which the high electron density can be attributed to lone-pair donation from the S atoms into the π-bonded system. Common acceptor units, meanwhile, typically feature electron withdrawing ketone, thiadiazole, ester and fluorine groups as found in diketopyrroloyrrole (DPP), thienopyrrolodione (TDP), benzothiadiazole (BT), 5,6-difluorobenzothiadiazole (ffBT) and thienothiophene (TT) that has appending fluorine and/or ester groups. The rest of this review will cover the D-A polymer structures that are currently demonstrating the highest efficiencies in BHJ organic solar cells, which have been broadly be categorized by their component D and A units. Only polymers found to give at least 8% PCE are discussed, as a rough benchmark for 'high efficiency', but the reader is referred to several other reviews for a more comprehensive account of donor polymer development if required [8,10,82,83].

3. Benzodithiophene polymers

3.1. Benzodithiophene-thienothiophene polymers

D-A polymers based on the benzo[1,2-b:4,5-b′]dithiophene (BDT) unit have undoubtedly been amongst the most successful in the last decade, now yielding efficiencies >10% in single junction and tandem devices [84–86]. The rigid, planar structure of fused rings in BDT affords a highly delocalized π-system that is beneficial for hole transport and for reducing the bandgap. In addition, the 4,8-positions allow for the incorporation of various side-chains on the central benzene ring. Starting from 3-carboxylic acid, a 3-step synthesis gives the BDT-dione intermediate, which can then be substituted with alkyl, aromatic or alkoxy groups as required. The fused thieno[3,4-b]thiophene (TT) ring system is frequently chosen as a co-monomer for BDT due to its ability to stabilize the quinoidal structure (Fig. 4), which has contributed to lowering the bandgap in many OPV polymers [87–90]. Substitution of an electron-withdrawing ester group affords acceptor character to the TT moiety, which further helps to lower the bandgap via molecular orbital hybridization. Representative BDT-TT based polymers (**P1–8**) and their device characteristics are shown in Fig. 5 and Table 1. Several D-A polymers were designed initially with the BDT-TT structure that gave moderate device performance [91–93], however the addition of a fluorine atom to the TT unit in **P1** (elsewhere known as PTB7) led to significantly higher efficiency devices of 7.4% [94]. The fluorine substituent had the effect of lowering the HOMO (−5.15 eV) but also the LUMO (−3.31 eV), resulting in a higher V_{OC} relative to the unsubstituted counterpart, whilst maintaining a high J_{SC} thanks to the narrow bandgap. A large wave of studies subsequently followed to investigate the fundamental device physics with this polymer and further optimize the performance [84], and a PCE of 9.2% was achieved by changing to an inverted device architecture [25]. Recently, conventional devices giving 10% PCE were reported with **P1** using a non-conjugated small molecule electrolyte to replace the Ca interlayer [95].

Another significant step was taken by replacing the alkoxy side-chains of **P1** with 2D-conjugated alkylthienyl groups (**P3**). This resulted in a deeper HOMO level and therefore a higher V_{OC}, as well as improved π-stacking, which contributed to a higher hole mobility and reduction in the optical bandgap. As such, efficiencies of up to 10.7% were possible with **P3** (otherwise known as PTB7-Th, PBDTTT-EFT or PCE-10) with $PC_{71}BM$ as the acceptor [24]. In addition, 8.7% PCE was achieved with the non-fullerene acceptor ITIC-Th, although in this case the efficiency was limited by the overlapping absorption spectra of the two materials [96]. Recently an off-center spinning method was used to deposit the active layer,

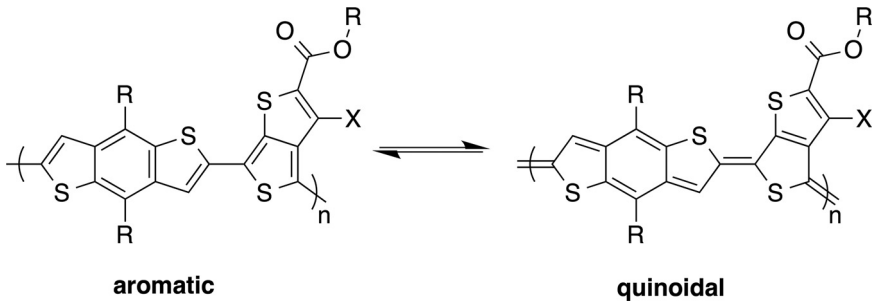

Fig. 4. Generic structure of BDT-TT polymer, wherein the thieno[3,4-b]thiophene (TT) unit helps to stabilize the quinoidal structure and planarize the backbone.

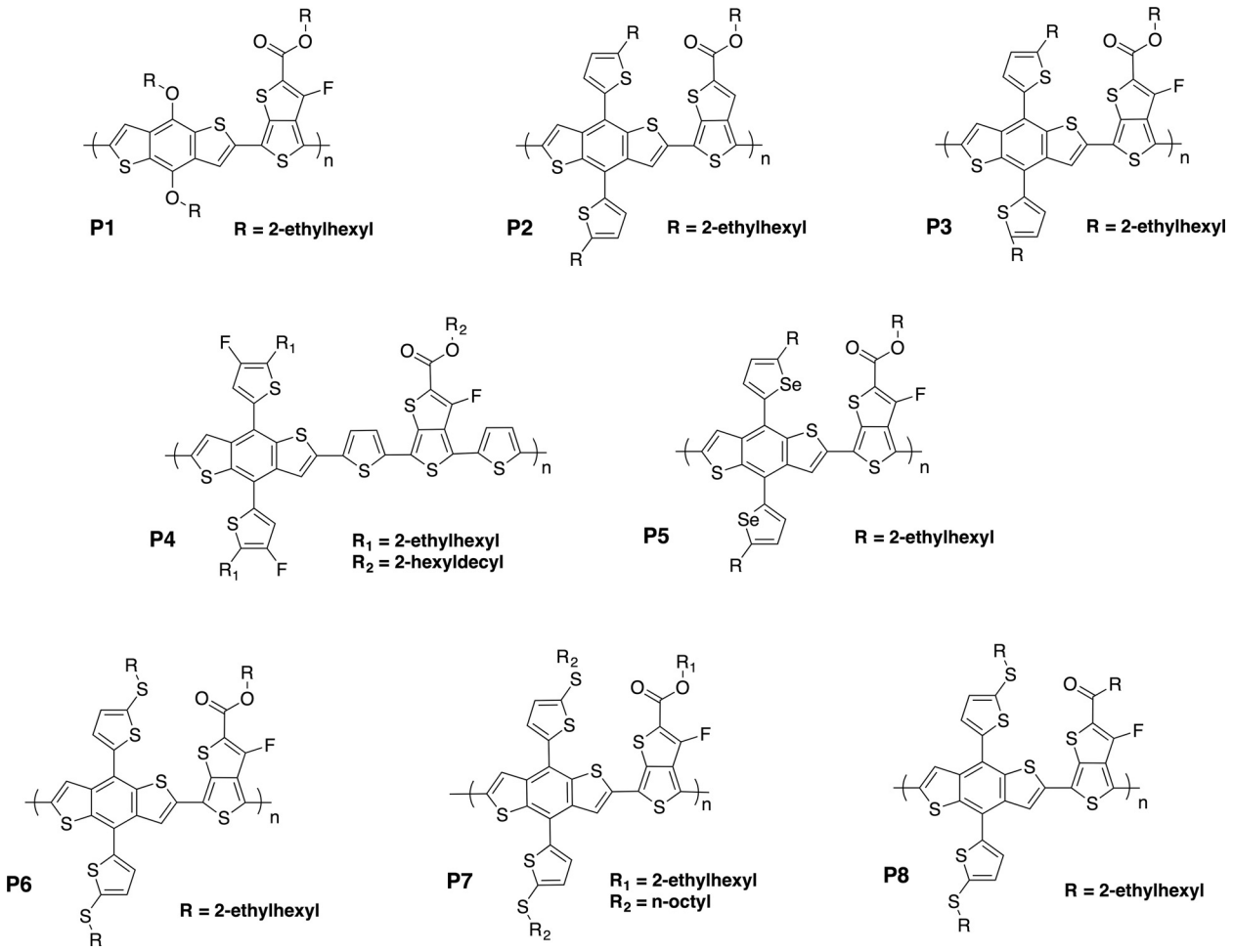

Fig. 5. Benzodithiophene-thienothiophene polymers with >8% efficiency.

Table 1
Benzodithiophene-thienothiophene polymers with >8% efficiency in single junction OPV devices.

	E_g^{opt} (eV)	IP (eV)	EA (eV)	Acceptor	additive	architecture	J_{SC} (mA cm^{-2})	V_{OC} (V)	FF	PCE (%)	Refs.
P1	1.64	5.15	3.31	$PC_{71}BM$	DIO	conventional	19.3	0.76	0.68	10.0	[95]
P2	1.58	5.10	3.25	$PC_{71}BM$	DIO	inverted	17.7	0.77	0.67	9.1	[99]
P3	1.58	5.20	3.56	$PC_{71}BM$	DIO	inverted	19.3	0.81	0.70	10.9	[97]
				ITIC-Th	CN	inverted	15.9	0.80	0.68	8.7	[96]
P4	1.64	5.20	3.30	$PC_{71}BM$	DIO	conventional	15.2	0.78	0.72	8.6	[101]
P5	1.60	5.19	3.25	$PC_{71}BM$	none	inverted	15.4	0.83	0.69	8.8	[104]
P6	1.57	5.41	3.27	$PC_{71}BM$	none	conventional	15.3	0.84	0.65	8.4	[107]
P7	1.51	5.33	3.52	$PC_{71}BM$	DIO	conventional	20.5	0.78	0.63	10.5	[111]
P8	1.56	5.44	3.31	$PC_{71}BM$	DIO	inverted	15.1	0.89	0.71	9.6	[112]

which apparently resulted in a more favorable vertical phase separation and efficiencies of nearly 11% were reported [97]. Similarly to **P1**, the fluorinated TT unit showed superior performance relative to the unsubstituted counterpart **P2** [98,99]. The effect of the fluorine substituent on the TT unit has been investigated systematically by varying the feed ratio of fluorinated and non-fluorinated TT monomer [100]. Within this study, it was found that reducing the fluorine content resulted in a higher-lying HOMO and therefore a reduced V_{OC}, as well as a reduction in fill factor due to the lower hole mobility and a less favourable, highly phase-separated morphology. From these results it appears that the fluorinated TT monomer is certainly beneficial to photovoltaic performance. In another study, fluorine atoms were added to the alkylthienyl side-chain on the BDT as well as the TT unit, in this case with a thiophene π-bridge included between the BDT and TT moieties (**P4**) [101]. A similar trend in V_{OC} was found, with a maximum PCE of 8.6% for the polymer with fluorine atoms in both positions. It has previously been observed that selenium substitution for sulfur in thiophene can yield higher charge carrier mobilities and reduced optical bandgaps in semiconducting polymers due to enhanced π-π interactions [102]. This has also been demonstrated for full backbone substitution in BDT-TT polymers, with a significantly higher J_{SC} obtained relative to the thiophene equivalent polymer [103]. Likewise, substitution of the alkylthienyl side-chains in **P3** with alkylselenophenyl groups (**P5**) was shown to result in stronger intermolecular interactions, which allowed for optimum device performance of 8.8% PCE to be achieved without any solvent additives [104]. Alkylfuranyl substituents, meanwhile, produced even stronger π-stacking due to the lower dihedral angle of the conjugated side-chain substituent, but in this case the intermolecular interactions were found to be too strong which resulted in excessive phase separation for the device [105]. Elsewhere, the alkyl chain on the conjugated alkylthienyl side-chains was replaced with an alkylthio group (**P6–8**). This resulted in a lower-lying HOMO energy for **P6**, in this case measured to be 0.1 eV lower than the alkylthienyl analogue **P3**. The moderate electron-acceptor character of alkylthio substituents has been previously attributed to the ability of divalent sulfur to accept π-electrons from the conjugated system into its empty 3d-orbitals, in contrast to alkoxy side-chains which are found to raise the HOMO by their electron-donating character [106,107]. The relatively large V_{OC} obtained in **P6** devices led to a moderate PCE of 8.4%, although it should be noted that the alkylthio substituents led to considerably decreased thermal stability [107]. Changing from branched to linear alkylthio side-chains (**P7**) led to significantly increased short circuit current values due to the stronger interchain π-π packing in this polymer [108,109], an effect that was further enhanced by using the regioregular polymer (10.2% PCE) over the regiorandom version (9.7%) [110]. An additional enhancement up to 10.5% PCE was obtained for **P7** by employing a novel hybrid structure of carbon nanotubes with a self-assembled molecule as the cathode interlayer [111]. Replacement of the ester side-chain on the TT unit with a carbonyl substituent, i.e. removing the electron-donating alkoxy group, led to an even lower-lying HOMO for **P8** and this resulted in a V_{OC} of 0.89 V.

3.2. Benzodithiophene-benzodithiophenedione polymers

Several polymers (**P9**–**13**) with >8% PCE have been published with BDT units co-polymerized with benzo[1,2-c:4,5-c′]dithiophene-4,8-dione (BDD), as shown in Fig. 6 and Table 2. The BDD acceptor can be synthesized in 4 steps in moderate yields [113], and allows for the incorporation of two alkyl chains for greater control over solubility. Compared to the BDT-TT polymers discussed in Section 3.1, BDT-BDD polymers tend to have wider bandgaps (1.8–1.85 eV) and therefore slightly reduced photocurrents, however the low-lying HOMO of this structure can produce V_{OC} values of >0.9 eV. In addition, the wider bandgap of these materials makes them ideal partners for lower bandgap, non-fullerene acceptors as a pathway to devices with both high V_{OC} and high J_{SC} values [33,96]. For example, the polymer **P9** gave 8.75% PCE with $PC_{61}BM$ as the acceptor, which is notably high for this fullerene with its limited visible wavelength absorption [114]. However, replacing $PC_{61}BM$ with the low bandgap small molecule acceptor ITIC resulted in efficient photocurrent generation between 300 and 800 nm thanks to the complementary absorption profiles of the materials, and as such devices achieved 11.2% PCE, as well as benefitting from improved morphological stability relative to the fullerene device [33]. **P9** also exhibited strong temperature-dependent aggregation in solution, which has been suggested to be helpful for the formation of pure polymer domains that have been shown to suppress non-geminate recombination [62,113,115]. Elsewhere, the BDT unit itself was modified to give the benzodifuran monomer seen in **P11**, for which the more electronegative oxygen atom resulted in a deeper HOMO and therefore larger V_{OC} relative to the thiophene equivalent **P10** [116]. Replacement of the sulfur atom on the BDD unit with selenium also yielded a large V_{OC} of 0.91 V for **P12**, when paired with a perylene diimide-based small molecule acceptor [117]. The relatively high hole mobilites in this case (2.6×10^{-3} cm^2 V^{-1} s^{-1}) were attributed to the more diffuse selenium electron cloud, which leads to increased Se-Se intermolecular interactions, however the lack of absorption beyond 700 nm may have limited the photocurrent in this case. An extended BDT monomer dithienobenzodithiophene was also introduced in **P13** in order to reduce conformational disorder and therefore improve the charge transport properties via the fused ring structure, resulting in 9.7% PCE with $PC_{71}BM$ [118]. This polymer showed similar performance with the non-fullerene acceptor ITIC-Th, with a slightly higher J_{SC} that can be attributed to the more complementary absorption of these materials [96]. Similarly to **P9**, this polymer also demonstrated significant aggregation behaviour in solution.

3.3. Benzodithiophene with other comonomers

2,1,3-Benzothiadiazole (BT) is a popular building block in semiconducting polymers because of its commercial availability and strong electron acceptor properties that can be further tuned by substitution at the 5,6-positions [119–121]. In addition, facile bromination at the 4,7-positions allows access to a variety of cross-coupling chemistry. Representative BT containing polymers (**P14–21**) and their device characteristics are shown in Fig. 7 and Table 3. Using Suzuki cross-coupling, the co-polymer of BDT with BT (**P14**) could be produced in large quantities via highly scalable flow synthesis techniques, yielding 9.5% PCE in devices [122]. It should be noted that two alkyl chains were appended to the thienyl group in this case, which allowed high molecular weight (>100 kg mol^{-1}) polymers to be synthesized despite the lack of solubilizing substituents on BT. Elsewhere, alkylated thiophene spacer groups have been used to ensure solubility (**P15–16**) [123]. Encouragingly, **P16** gave optimum device performance without any solvent additives or post-treatment, and a minimal loss in efficiency was observed for thicker films up to 300 nm, both of which are favourable for roll-to-roll printing applications. **P17** also formed an optimum morphology without solvent additives, although thermal annealing was used in this case to promote reorganization of the polymer [124]. In addition, the >8-step synthesis of this benzotriazole based monomer is not ideal for large-scale fabrication. By contrast, the difluorobenzotriazole monomer used in **P18** was synthesized more easily in 4 steps [40]. The 1.9 eV bandgap of this polymer made it an ideal partner for the low bandgap, small molecule acceptor ITIC, resulting in efficient photocurrent generation between 300 and 800 nm and promising efficiencies of 9.5%. Linear alkylthio side-chains on the

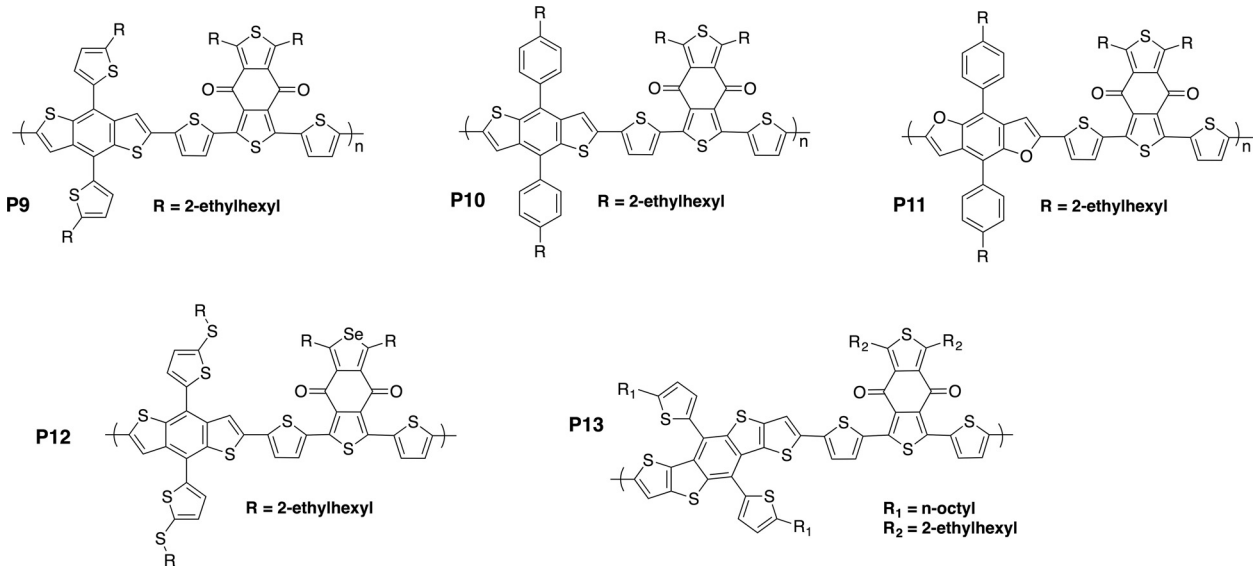

Fig. 6. Benzodithiophene-benzodithiophenedione polymers with >8% efficiency.

Table 2
Benzodithiophene-benzodithiophenedione polymers with >8% efficiency in single junction OPV devices.

	E_g^{opt} (eV)	IP (eV)	EA (eV)	Acceptor	Add −itive	Arch −itecture	J_{SC} (mA cm^{-2})	V_{OC} (V)	FF	PCE (%)	Refs.
P9	1.80	5.33	2.92	$PC_{61}BM$	DIO	conventional	14.3	0.88	0.70	8.8	[114]
				ITIC	DIO	inverted	16.8	0.90	0.74	11.2	[33]
P10	1.81	5.43	3.52	$PC_{71}BM$	DIO	conventional	13.1	0.86	0.72	8.1	[116]
P11	1.83	5.32	3.52	$PC_{71}BM$	DIO	conventional	13.3	0.92	0.77	9.4	[116]
P12	1.85	5.34	3.53	SdiPBI-S	DIO	conventional	12.8	0.91	0.69	8.2	[117]
P13	1.85	5.36	3.43	$PC_{71}BM$	DIO	conventional	14.1	0.92	0.75	9.7	[118]
				ITIC-Th	CN	inverted	16.2	0.88	0.67	9.6	[96]

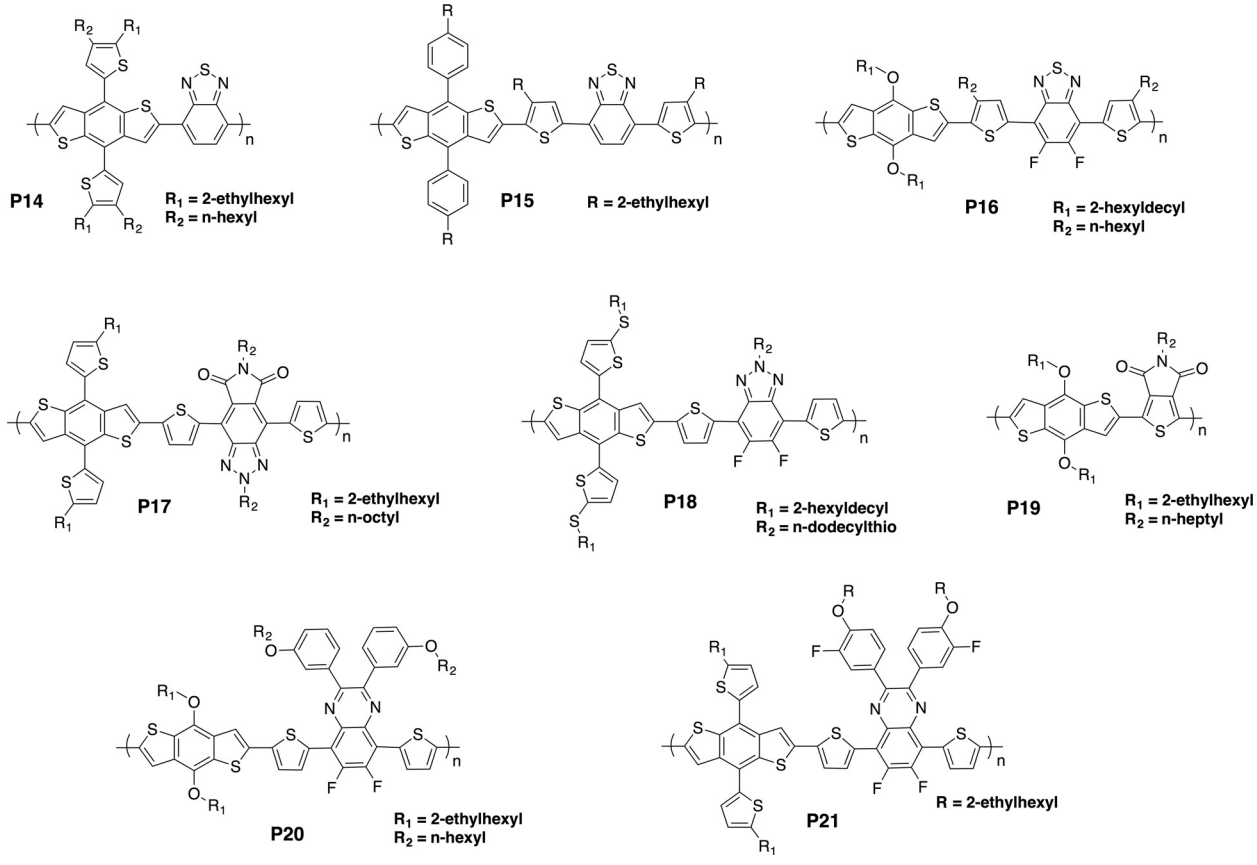

Fig. 7. Benzodithiophene polymers with other comonomers giving >8% efficiency.

Table 3
Other benzodithiophene polymers with >8% efficiency in single junction OPV devices.

	E_g^{opt} (eV)	IP (eV)	EA (eV)	Acceptor	Addit –ive	architecture	J_{SC} (mA cm^{-2})	V_{OC} (V)	FF	PCE (%)	Refs.
P14	1.75	5.45	3.70	$PC_{71}BM$	none	inverted	15.7	0.92	0.66	9.5	[122]
P15	1.70	5.35	3.34	$PC_{71}BM$	DIO	conventional	12.9	0.88	0.71	8.1	[123]
P16	1.70	5.31	3.20	$PC_{71}BM$	none	conventional	15.4	0.78	0.69	8.3	[132]
P17	1.81	5.34	3.46	$PC_{71}BM$	none	conventional	13.5	0.87	0.74	8.6	[124]
P18	1.93	5.32	3.08	ITIC	none	conventional	17.4	0.89	0.61	9.5	[40]
P19	1.80	5.56	3.75	$PC_{71}BM$	CN	conventional	12.6	0.97	0.70	8.5	[125]
P20	1.73	5.52	3.30	$PC_{71}BM$	DIO	conventional	18.2	0.76	0.58	8.0	[128]
P21	1.70	5.36	3.56	$PC_{71}BM$	DIO	conventional	14.5	0.85	0.70	8.6	[129]

BDT unit were found to promote stronger interchain π-π stacking in this case, which may account for the more favorable morphology that was obtained without solvent additives. Other acceptor units that have successfully been incorporated into BDT polymers with >8% PCE include thienopyrroledione (TPD), as demonstrated in **P19** [125–127], and difluoroquinoxaline (**P20–21**) [128,129]. Fluorine substitution is widely used in D-A polymers as a way of improving the active layer morphology and charge carrier mobility due to the inter- and intramolecular interactions that arise from the induced dipole at the fluorine [82,130,131]. The same principle was applied for **P20**, although in this case it was not reflected in a particularly high FF. For **P21**, fluorine atoms were also introduced at the meta position of the alkylphenyl substituents, which may have contributed to the higher FF devices.

4. Oligothiophene polymers

As discussed in Section 2.6, the planar backbone of the thiophene polymer P3HT, and the highly ordered lamellar and π-stacking properties that benefit from this, have made P3HT one of the most widely used polymers in organic electronics. Recently, the alkylated oligothiophene (bi-, ter- and quaterthiophene) segments have become increasingly popular in D-A polymers (**P22–33**, Fig. 8 and Table 4). Arguably the most influential contribution in this area was the publication of three alkylated quaterthiophene donor polymers giving >10% PCE with multiple different fullerenes [62]. The high performance for all three polymers (**P22–24**) was attributed to the strong temperature-dependent aggregation properties (Fig. 9a). Since the polymer is already partially aggregated in solution prior to spin-casting, this can encourage the formation of very pure and crystalline domains during film formation, as has been observed for similar structures elsewhere [133–135]. In this case, the highly ordered but small domains contributed to high hole mobilities ($1.5–3 \times 10^{-2}$ cm^2 V^{-1} s^{-1}) with minimal charge recombination. This allowed for a high FF to be achieved with relatively thick (300 nm) active layers. As shown in Fig. 9b, this increased thickness was beneficial in terms of light absorption, with a 30% higher J_{SC} obtained relative to 150 nm films. Thicker films are also more practical for industrial applications due to the greater roughness tolerance and ease of deposition, which makes this a promising development for OPV scale-up. By contrast, the optimum film thickness for devices with most BDT-TT polymers is around 100 nm [86], which may be related to the relatively amorphous, impure polymer domains that are characteristic of these blends [50,52]. As discussed in Section 2.5, domain purity has been shown to be important for charge transport and to minimize recombination in thicker films [59,60,136,137]. The chain length and branching point in polymers **P22–24** was found to be critical in determining the length scale of phase separation during film formation, as is the case for many D-A polymers [138–140]. Polymers with 1-position branching demonstrated no aggregation in solution and therefore produced films with poor crystallinity, whereas 3-position branching resulted in excessive aggregation even in warm solutions, resulting in films that gelled immediately upon spin-casting. Meanwhile, increasing the chain length to 2-decyltetradecyl (**P25**) led to a reduction in average domain purity and crystallinity, as well as a slight reduction in absorption coefficient due to the larger fraction of non-absorbing alkyl chains in the film, both of which may contribute to the poorer device performance [62,133,141]. However, longer chains were also found promote face-on orientation of the polymer, which is known to be beneficial for charge transport OPV devices [142–144]. To balance these factors, the intermediate chain 2-nonyltridecyl (**P26**) was introduced. This polymer demonstrated an even higher efficiency of 11.7% when processed from non-halogenated solvents, which is greatly encouraging for the development of more environmentally friendly and industrially applicable OPV [145]. It should also be noted that **P22** has demonstrated high efficiencies in blade-coated devices, a technique that can be seen as a prototype for the more scalable and industrially applicable slot-die coating [63]. Interestingly, the blade-coated device performance was comparable to the spin-coated device despite the different morphology obtained (edge-on orientation with bimodal phase separation), supporting the idea that there is no 'ideal' morphology in OPV, but multiple different morphologies that can lead to high performance. Modification of the fluorinated benzothiadiazole (ffBT) acceptor unit has also been explored. **P27** replaces this with difluorobenzoxadiazole (ffBX), which leads to a 0.1 eV increase in V_{OC} thanks to the lower-lying HOMO energy associated with the more electronegative oxygen atom [146]. However, the reduced active layer thickness in this case was found to limit the J_{SC} compared to ffBT devices. It should also be noted that the synthesis and bromination of BX derivatives is considerably more complex relative to BT [146,147]. An improved V_{OC} of 0.93 V was also obtained using the structural isomer of ffBT difluorobenzo[d][1,2,3]thiadiazole (**P28**) [141]. Elsewhere, BDD has instead been used as the electron deficient unit, along with fluorinated thiophene spacer groups (**P29**). This polymer gave efficiencies over 9% with $PC_{71}BM$ as the acceptor [148], as well as comparable OPV performance with the non-fullerene acceptor ITIC [149]. As an alternative strategy to lower the HOMO, carboxylate substituents at the 3-position of the thiophene have been shown to increase the V_{OC} (**P30–31**) [150,151]. Interestingly, it was found that blends of terthiophene polymer **P31** with a non-fullerene acceptor SF-PDI_2 could achieve high efficiencies despite having a negligible driving force for charge separation. This small energy offset, combined with low rates of bimolecular recombination, resulted in much smaller voltage losses compared to typical OPV devices so that a V_{OC} of 1.11 V could be achieved. Another terthiophene polymer, this time with an asymmetric arrangement of alkyl chains on the backbone (**P32**), gave efficiencies of 10.7% without DIO. This promising result indicates that decreasing the ratio of thiophenes to ffBT units along the backbone may be beneficial for moving towards additive-free processing. Meanwhile, the bithiophene polymer **P33** was synthesized wherein diketopyrrolopyrrole (DPP) was co-polymerized with ffBT as a second acceptor unit [152]. The strong electron deficient nature of DPP contributed to significantly lowering the bandgap to 1.43 eV, enabling a high J_{SC} of 18 mA cm^{-2} despite the relatively thin active layer (100 nm). **P33** was also reported to offer good air stability,

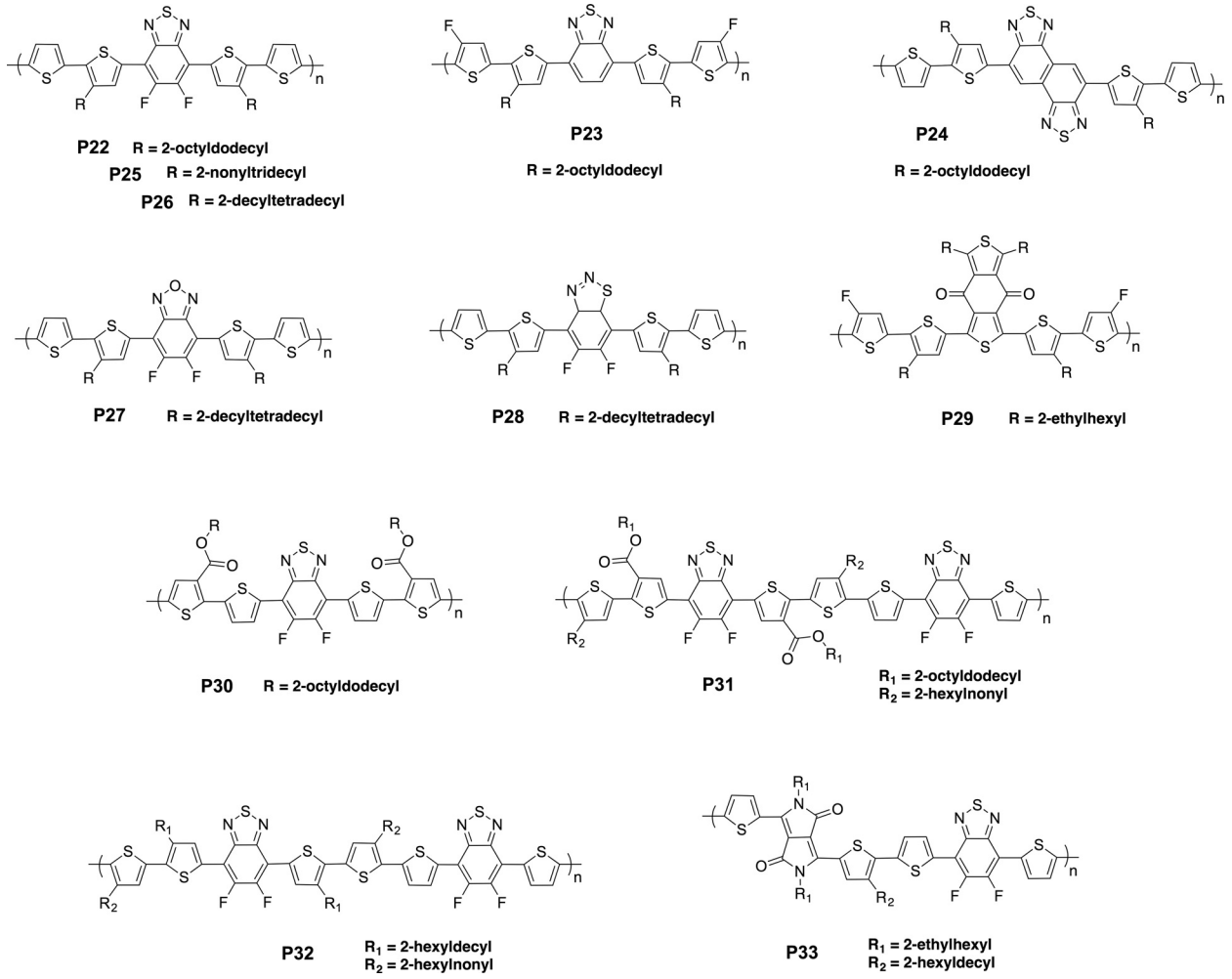

Fig. 8. Oligothiophene polymers with >8% efficiency.

Table 4
Oligothiophene polymers with >8% efficiency in single junction OPV devices.

	E_g^{opt} (eV)	IP (eV)	EA (eV)	Acceptor	Add- itive	Architecture	J_{SC} (mA cm^{-2})	V_{OC} (V)	FF	PCE (%)	Refs.
P22	1.65	5.34	3.69	$TC_{71}BM$	DIO	inverted	18.8	0.77	0.75	10.8	[62]
P23	1.63	5.20	3.57	$PC_{71}BM$	DIO	inverted	18.2	0.77	0.74	10.4	[62]
P24	1.53	5.24	3.71	$PC_{71}BM$	DIO	inverted	19.8	0.76	0.68	10.1	[62]
P25	1.66	5.50	3.90	$PC_{71}BM$	DIO	conventional	16.5	0.76	0.71	8.8	[141]
P26	–	–	–	$PC_{71}BM$	PN	inverted	20.4	0.78	0.74	11.7	[145]
P27	1.66	5.51	3.85	$PC_{71}BM$	DIO	inverted	13.8	0.88	0.68	9.4	[146]
P28	1.80	5.70	3.80	$PC_{71}BM$	DIO	conventional	13.1	0.93	0.74	9.0	[141]
P29	1.74	5.42	3.53	$PC_{71}BM$	none	conventional	13.6	0.95	0.75	9.2	[153]
				ITIC	DPE	inverted	15.0	0.94	0.61	8.7	[149]
P30	1.77	5.72	3.95	$PC_{71}BM$	DIO	conventional	14.9	0.87	0.71	9.3	[150]
P31	1.72	5.37	3.57	SF-PDI_2	ODT	inverted	13.3	1.11	0.64	9.5	[151]
P32	1.63	5.31	3.68	$PC_{71}BM$	none	inverted	18.9	0.82	0.69	10.7	[154]
P33	1.43	5.33	3.62	$PC_{71}BM$	DIO	inverted	18.0	0.82	0.62	8.6	[152]

with a minimal drop in efficiency after 30 days shelf storage, as well as maintaining a stable morphology with high temperature annealing. While this is advantageous, it should be noted that stability studies were not found for the other device data reported in Table 4, and there is evidence that devices with **P22** may be quite unstable [39]. It is also worth mentioning that the temperature-dependent aggregation of these polymers, while beneficial in terms of morphology, may create barriers to scale-up due to engineering difficulties associated with the elevated and very specific temperature range required for deposition.

5. Other >8% PCE polymers

Several other D-A polymers have demonstrated promising OPV performance with efficiencies >8% (**P34**–**39**, Fig. 10 and Table 5). The strong electron deficient nature of diketopyrrolopyrrole (DPP) is responsible for significantly stabilizing the LUMO in **P34**, resulting in a low bandgap of 1.39 eV [155]. However, the V_{OC} is limited in this case due to the lack of HOMO stabilization. The bandgap is further reduced by exchanging the bridging thiophene for selenophene (1.37 eV) and tellurophene (1.32 eV), due to the reduction in aromaticity with increasing chalcogen atom size, although this also

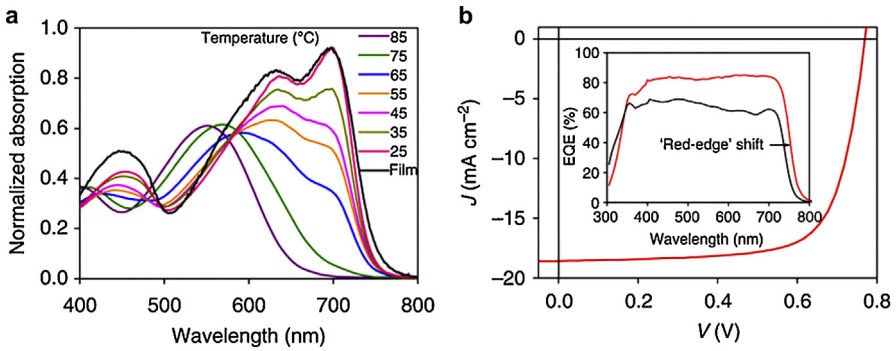

Fig. 9. (a) UV-vis spectra of P22 in solution at different temperatures, demonstrating temperature dependent aggregation; (b) J-V curve and EQE (inset) for P22 devices at 150 nm (black) and 300 nm (red) thickness. [62], Copyright 2014, Adapted with permission from the Nature Publishing Group.

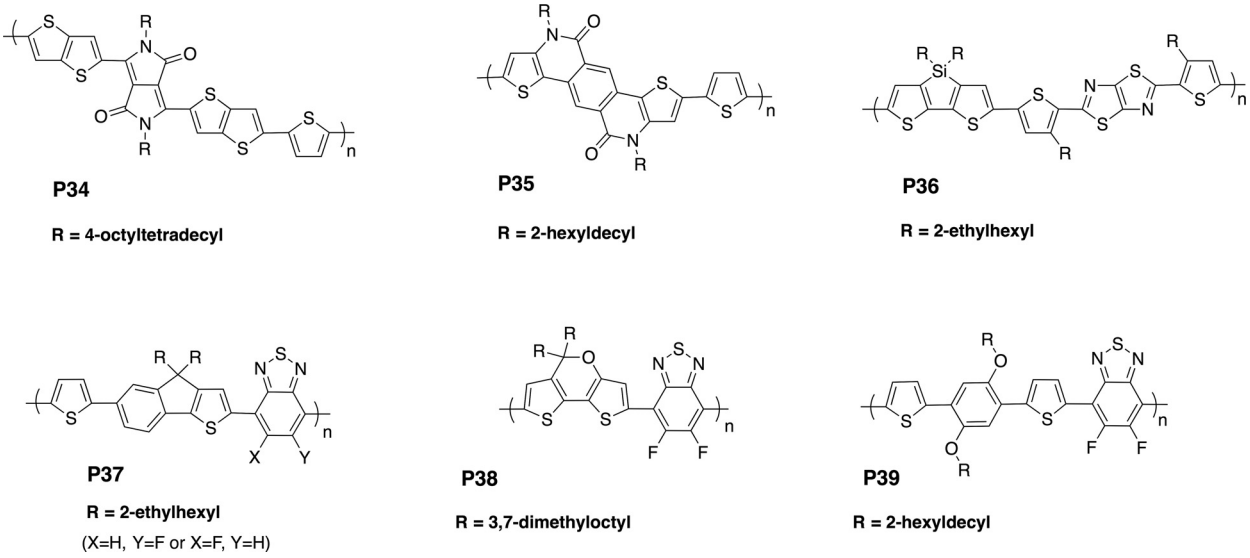

Fig. 10. Other D-A polymers with >8% efficiency.

Table 5
Other polymers with >8% efficiency in single junction OPV devices.

	E_g^{opt} (eV)	IP (eV)	EA (eV)	Acceptor	Add −itive	Architecture	J_{SC} (mA cm^{-2})	V_{OC} (V)	FF	PCE (%)	Refs.
P34	1.39	5.08	3.69	$PC_{71}BM$	none	inverted	23.5	0.57	0.66	8.8	[155]
P35	1.86	5.40	2.80	$PC_{71}BM$	DIO	inverted	14.3	0.88	0.73	9.2	[158]
P36	1.77	5.10	3.30	DBFI-EDOT	none	conventional	13.8	0.93	0.63	8.1	[160]
P37	1.82	5.50	3.68	$PC_{71}BM$	DPE	conventional	15.4	0.90	0.66	9.1	[161]
P38	1.38	5.26	3.64	$PC_{71}BM$	none	conventional	18.0	0.70	0.63	8.0	[162]
P39	1.76	5.45	3.69	$PC_{71}BM$	DPE	conventional	16.3	0.79	0.73	9.4	[130]

further reduces the V_{OC}. The pentacyclic lactam acceptor used in **P35** results in a wider bandgap material that has a significantly lower J_{SC}, but balanced by a larger V_{OC} from the deeper HOMO [156,157]. The thiazolothiazole-dithienosilole polymer **P36** has demonstrated promising device performance with both fullerene and non-fullerene acceptors [158–160], although the photocurrent in the best performing cells (DBFI-EDOT acceptor) may have been limited by the relatively narrow absorption of **P36** [160]. Elsewhere, 9.1% PCE was demonstrated with the polymer **P37**, which incorporates an asymmetric indenothiophene donor moiety co-polymerized with monofluorinated BT, challenging the idea that symmetric monomers are important for high performance [161]. Other BT based polymers include **P38**, which introduces a dithienopyran (DTP) donor building block [162]. The electron-donating oxygen in the pyran ring afforded DTP a high-lying HOMO as well as strong D-A intramolecular interactions with the ffBT co-monomer, both of which contributed to the small bandgap of 1.38 eV. **P38** also improved solubility relative to other commonly used donor units, allowing high molecular weights to be obtained using less bulky side-chains (3,7-dimethyloctyl). Finally, the ffBT polymer **P39** was designed to take advantage of the planarizing effects of non-covalent, intramolecular interactions along the backbone [130]. Facilitating non-bonding interactions such as dipole-dipole interactions, H-bonding and attractive N···H, F···S or O···S interactions has been widely demonstrated as an effective strategy to reduce backbone torsion whilst maintaining good solubility [82,163–167]. In the case of **P39**, the dialkoxyphenylene building block allows for seven possible attractive interactions (N···H, N···S, F···H, F···S, F···H, O···H and O···S), as depicted in Fig. 11. This afforded a highly planar backbone with tight interchain packing, which in turn led to the formation of a highly ordered, nanofibrillar network morphology with balanced electron

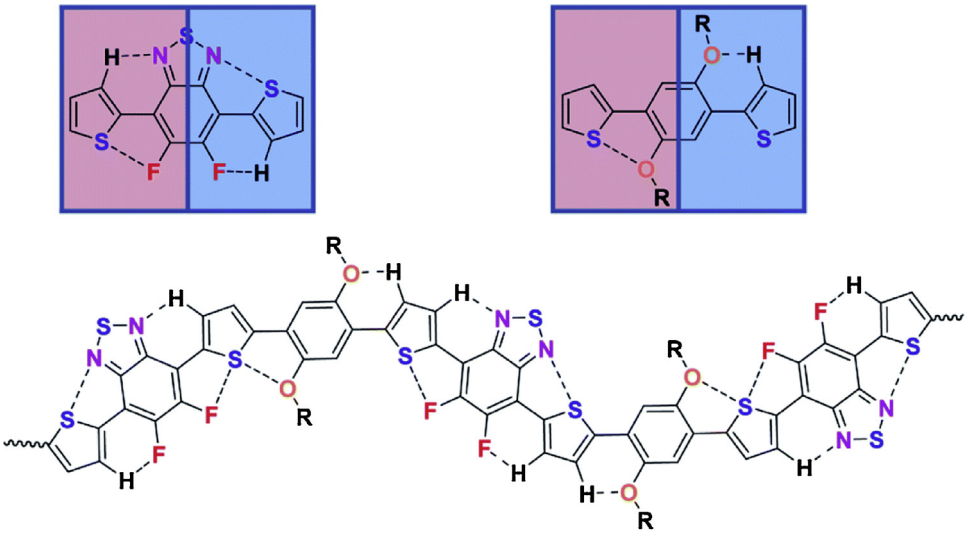

Fig. 11. Proposed non-covalent interactions planarizing the polymer chain of P39. [130], Copyright 2014, Adapted with permission from the Royal Society of Chemistry.

and hole mobilities, allowing for optimum solar cells performance in thick (290 nm) films. This 'conformational locking' strategy holds great promise for developing planar, highly ordered materials that remain highly soluble, and fortunately it is also attracting increasing attention in the theoretical community to understand the nature of these interactions and predict their effects [168].

6. Cost-effectiveness in OPV

One of the main attractions of OPV is the potential for low-cost solar energy. However, despite a rapid development in the performance of OPV, the cost-effectiveness of this technology is still questionable and there have been relatively few publications addressing the question of how to reduce the overall cost of this technology. In terms of fabrication, the solution processed techniques used in OPV already offer a significant advantage relative to traditional vacuum deposition techniques used for inorganic solar cells. For materials costs, the organic semiconductors and electrodes must of course be considered, as well as any additional electron- and hole- transport layers. It was estimated in 2007 that the cost of a photovoltaic system should be less than $\$10\,m^{-2}$ in order for solar energy to compete with fossil fuels for primary energy consumption [169]. However, the current cost of OPV modules, considering only the active layer materials (not the electrodes, interlayers, substrates, encapsulants *etc*) still exceeds this. If we consider the current average market prices for the traditional active layer blend of P3HT and $PC_{61}BM$ (mass ratio: 1:1, layer thickness: 200 nm), the cost of P3HT (market price: $\sim\$300\,g^{-1}$, density: $\sim1.1\,g\,cm^{-3}$) is $\sim\$51\,m^{-2}$ and the cost of $PC_{61}BM$ (market price: $\sim\$400\,g^{-1}$, density: $\sim1.5\,g\,cm^{-3}$) is $\sim\$38\,m^{-2}$, resulting in a cost of $\sim\$89\,m^{-2}$ for the active layer. Looking instead at higher performance materials, for example PTB7 and $PC_{71}BM$ (mass ratio: 1:1.5, layer thickness: 100 nm), the cost of PTB7 (market price: $\sim\$2000\,g^{-1}$, density: $\sim1.1\,g\,cm^{-3}$) is $\sim\$148\,m^{-2}$ and the cost of $PC_{71}BM$ (market price: $\sim\$900\,g^{-1}$, density: $\sim1.5\,g\,cm^{-3}$) is $\sim\$44\,m^{-2}$, which results in a total cost of $\sim\$192\,m^{-2}$.

Estimation of material cost in $\$\,m^{-2}$ is calculated as follows:

$$\text{Material 1 (Polymer)}: \text{cost} = (\text{thickness}) \times \left(\text{price/g}\right) \times \left(\frac{\text{density1} \times \text{density2}}{\text{mass ratio} \times \text{density1} + \text{density2}}\right)$$

$$\text{Material 2 (fullerene)}: \text{cost} = (\text{thickness}) \times \left(\text{price/g}\right) \times \left(\frac{\text{mass ratio} \times \text{density1} \times \text{density2}}{\text{mass ratio} \times \text{density1} + \text{density2}}\right)$$

It should be noted that the bulk prices for manufacture should be considerably lower than current market prices, as has been estimated elsewhere [170], however it is clear that the cost of high performance active layer materials is prohibitively high at this stage.

A more comprehensive analysis of manufacturing costs for OPV modules was published in 2009 [171]. In this report, the levelized cost of electricity (LCOE) of an OPV module was calculated between 49 ¢/kWh and 85 ¢/kWh under the assumption of 5% efficiency and 5-year lifetime, which was consistent with the low efficiency and stability of OPV at that time. More recent calculations indicate that the LCOE of mass-manufactured OPV modules could be as low as 10–13 ¢/kWh in future decades due to improvements in the manufacturing process as well as the materials production [172–175]. However, in order to really compete with fossil fuels as well as traditional silicon solar cells, the LCOE of OPV needs to be as low as 7 ¢/kW, which in turn requires the efficiency and lifetime to rise to 15% and 15–20 years, respectively. Considering the present record OPV module efficiency of 9.7% [176] and their relatively short-term stability, it would appear that OPV technology in its current stage is still very young and significant improvements are still needed for mass manufacture.

One important factor in the cost of OPV is the use of toxic reagents and solvents during both the synthesis of organic semiconductors and manufacture of the devices. Halogenated solvents such as chlorobenzene, 1,2-dichlorobenzene and DIO are typically used in OPV device fabrication due to their ability to effectively dissolve most of the organic semiconductors in question as well as their suitable boiling point and vapor pressure for promoting an optimal BHJ morphology. However, these solvents are relatively expensive to produce as well as adding to the production costs because of the extra steps required for safe handling and disposal of these toxic and environmentally hazardous materials. To directly circumvent this issue, it is important to explore alternative, more environmentally benign solvent systems based on non-halogenated, non-aromatic or even alcohol-based solvents, and also to consider tailoring the structures, in particular the side-chains, of these polymers to increase their solubility in such solvents [177,178]. There have recently been some highly encouraging results published in this area, both in terms of using

non-halogenated solvents in the polymer synthesis [179] and in device fabrication. Power conversion efficiencies over 8% have now been achieved in several instances using non-halogenated solvents and additives [180–183], and even the present record PCE for a single junction OPV (11.7%) was achieved using hydrocarbon solvents (1,2,4-trimethylbenzene with 1-phenylnapthalene as a solvent additive) [145], offering a very encouraging signal that the field is moving now in this direction.

Besides solvents, another important aspect of production costs entails synthesizing the semiconducting polymers. For many of the high performance polymers in the literature, including the majority of >10% PCE polymers, their synthesis entails highly toxic organotin and highly flammable organolithium reagents, as well as synthesis routes that are often complex with over 10 steps and low yields of 1–5% [24,33,62,110,145,154]. For mass manufacture of OPV, this issue of synthetic complexity is therefore likely to become increasingly important. In an earlier report on the cost of OPV materials and their commercial viability, the number of synthetic steps was correlated with the total cost of a material by taking into account the costs of reagents, solvents, work-up and purification [170]. A linear relation was given (Fig. 12a), indicating a typical bulk material cost of \$31 g^{-1} $step^{-1}$ for the organic semiconductors considered. Another recent review discussing the synthetic complexity of OPV materials evaluated the total cost in terms of synthetic steps, cost of raw materials, reaction yields, purification steps and safety of reagents [184]. A figure of merit (FOM) was derived to describe the cost-effectiveness of certain OPV polymers that takes into account both the synthetic complexity (on a scale of 1–100) and efficiency of the corresponding devices, as shown in Fig. 12b. It is noted that P3HT has the lowest FOM of the materials studied, while the more complex D-A polymer structures have a high FOM primarily due to the larger number of synthetic steps. Some important steps have been taken to try to develop more efficient synthetic methods for polymer production, such as through the use of controlled polymerization methods [185,186], C-H activation chemistry to reduce the number of synthetic steps and avoid the use of toxic organotin reagents and/or unstable boronic esters [187,188], the use of natural products as precursors[189] and the development of more efficient and scalable techniques such as flow synthesis [190]. These promising results should be taken as inspiration for chemists to develop high performance D-A polymers using more efficient, environmentally friendly and cost-effective routes.

7. Efficiency limits in OPV

Although the efficiency of OPV devices has steadily increased and has now surpassed 10% PCE, the efficiency limit of OPV devices is still under active debate since the exact mechanism of photovoltaic processes, as well as the relationship between the device architecture and performance, are still not fully understand. For calculating the detailed balance limit (efficiency limit calculated using the Shockley-Queisser approach) of OPV devices, thermodynamic approaches with or without kinetic consideration according to Shockley-Queisser (SQ) theory, have been applied. In both approaches, the charge transfer (CT) state formed between the donor and the acceptor has been extensively studied and proven to play an important role in device properties [191–193]. Vandewal and others have applied the aspect of electronic transport to the SQ theory and revealed a reciprocal relationship between the quantum efficiency for current extraction and the quantum efficiency for electroluminescence of solar cells, which helps to rationalizes the open-circuit voltage (V_{OC}) loss and further the efficiency loss in OPV devices [194–196].

The thermodynamic approach was directly justified by the observations of CT states in OPV devices. Kirchartz et al. estimated an efficiency limit of ~23% for BHJ solar cells from this approach [197]. Their results also indicated that the low efficiency of BHJ solar cells is predominantly caused by the energy loss from non-radiative recombination at the donor and acceptor interface. Meanwhile, a dilemma for state-of-the art BHJ solar cells was stated in their report, suggesting that efficient quenching of photoluminescence of donor facilitates exciton dissociation at the donor-acceptor interface but significantly increases the rate of radiative recombination. Giebink et al. took a similar approach and related the free energy of charge transfer ($\Delta G_{CT} < 0$) to the efficiency limit of BHJ solar cells [198]. For current state of the art BHJ solar cells with $-\Delta G_{CT} = 0.3$ eV, the efficiency limit is ~27%. In addition, it is theoretically possible for BHJ solar cells to reach SQ limit if $-\Delta G_{CT} = 0.1$ eV is given. According to a detailed empirical study of CT state in BHJ solar cells by Veldman et al., there are three approaches to achieving a low $-\Delta G_{CT}$ [199]. One is minimizing the difference between the HOMO of donor and LUMO of acceptor. Another is enlarging the band gap of donor. The other is increasing the dielectric constant of donor to reduce the Coulomb energy of the CT exciton. Koster et al. [200] and Gruber et al. [201] discussed the role of CT exciton in BHJ solar cells. They suggested that although the CT state in BHJ solar cells leads to predominantly non-radiative recombination and causes low efficiency, OPV devices could still achieve over 30% PCE in the case where CT exciton exhibit either a very weak absorption or a strong absorption. A weak absorption helps to decrease V_{oc} loss while a strong one allows to increase J_{sc} by collecting additional photons.

The above thermodynamic approaches are based on the assumption of quasi-thermal equilibrium of charges in different energy states, which do not consider the kinetic limitation of the dissociation of CT exciton. Therefore, in order to achieve a more accurate, detailed balance limit of OPV devices, the kinetic processes should also be considered. The first attempt to apply kinetic limits to a thermodynamic approach on estimating the efficiency limit of OPV devices was made by Nelson and co-workers [202,203]. The authors presented a model based on a two-level, light absorbing system, connected to external electrodes by chains of charge transporting orbitals, deriving an expression governing the steady-state current-voltage characteristic of OPV devices using a generalized Planck equation for photon absorption and emission and Marcus theory for electron transfer. In this way, a detailed balance limit of ~20% was proposed for OPV devices. A purely kinetic approach was elsewhere applied and similar results were found as for the thermodynamic approach, suggesting that an efficiency limit, highly dependent on ΔG_{CT} and efficiency, close to SQ limit is possible for OPV devices [204]. Alongside several efforts to find the detailed balance limit of OPV devices, empirical approaches also provide a method with fewer physical theories and use simple calculations to estimate the practical limit of OPV devices. The derivation of the practical limit primarily includes an empirical equation that correlates V_{OC} to the donor and acceptor energy levels, and presumed values of external quantum efficiency (EQE) and fill factor (FF). Scharber et al. made one of the first, most critical contributions to studying the practical limit of OPV devices (using $PC_{61}BM$ as the acceptor) and proposed several quantitative rules for designing donors in BHJ solar cells [4]. These guidelines suggested that an efficiency of ~10% could be achieved with a donor LUMO level 0.3 eV higher than that of $PC_{61}BM$ and a band gap at ~1.5 eV for the donor, accompanying a constant EQE and FF of 0.65. Recently, Scharber modified this empirical approach by increasing the maximum EQE and FF to 0.70, raising the practical limit to ~13%; this is in line with the many high-performance BHJ solar cells fabricated with efficiencies over the initial calculation in the last decade [205]. Similar empirical approaches have been proposed elsewhere, with different empirical equations employed for V_{OC}, all suggesting practical limits within the range of 10–15% [199,206,207]. These

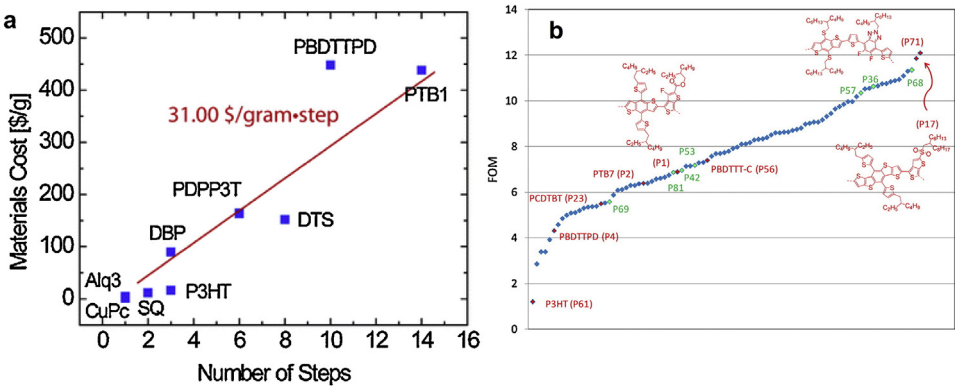

Fig. 12. (a) Relationship between number of synthetic steps for OPV materials and their cost (including estimated work-up/purification costs). [170], Copyright 2013, Adapted with permission from the Royal Society of Chemistry; (b) Figure-of-merit (FOM) of OPV polymers arranged in ascending pattern. [184], Copyright 2014, Adapted with permission from the American Chemical Society.

studies suggested that low values of $-\Delta G_{CT}$ (<0.5 eV) are desired for high-efficiency OPV devices, which is consistent with the results obtained from the calculation for detailed balance limit.

8. Conclusions and outlook

In the last few years, many new polymer structures have been developed for OPV that give >8% PCE, and even >10% PCE devices. In addition, several of the polymers that were developed in earlier years are now reported with significantly higher efficiencies than their original values, reflecting how important the developments in device architecture, materials and processing conditions have been for performance. Improved electron acceptor materials have been a significant part of this, with almost all of the high efficiency devices discussed in this review using $PC_{71}BM$ as the acceptor as opposed to the more traditional $PC_{61}BM$. In addition, the emerging popularity of small molecule acceptors that have intense absorption in the visible and near-IR part of the spectrum, as well tunable LUMO energies, may influence the way that donor polymers are designed in the future. For the D-A polymers discussed in this review, much of the focus has been on reducing the bandgap of the polymer whilst increasing the V_{OC}, normally with some compromise made between the two. However, low bandgap acceptors now offer the opportunity for wider bandgep (1.8–1.9 eV) polymers to be used alongside these acceptors, achieving simultaneously the broad absorption needed to maximize the photocurrent, whilst maintaining a large V_{OC}. The recent exploration of systems with very low voltage losses can also contribute to this. Polymers based on benzodithiophene donors, in particular BDT-TT structures with alkylthienyl and thioalkylthienyl substituents, remain some of the best performing polymers, with increasingly high efficiencies published every year thanks to improvements in processing and cell design. However, the recent emergence of consistently high performing oligothiophene polymers is certainly impacting on the OPV landscape. The temperature-dependent aggregation properties that many of these polymers share, in the presence of a second-position branched alkyl chain between the thiophene rings, is shaping a new paradigm in the 'ideal' morphology of BHJ devices. Whereas the most common BDT-TT blends are characterized by relatively amorphous polymer domains that have a large degree of miscibility with the fullerene, the high efficiency oligothiophene blends are characterized by very crystalline and pure, but also sufficiently small, polymer domains. Importantly, this morphology appears to be much more compatible with thicker films, allowing for >300 nm films to be made without a significant reduction in FF. This is significant for increasing the light harvesting of the device, but also for transferring to industrial printing processes, for which thicker films are necessary. On the other hand, the need to deposit these polymers from warm solution in order to achieve the appropriate morphology could create barriers for scale-up. It should also be noted that most of the high efficiency data reported in the literature is for small-scale devices with active areas typically <1 cm^2, whereas much larger areas are needed for industrial production. For this technology to be commercially viable, is also important that the materials can be produced on a large scale, with a minimum number of synthetic steps. The use of toxic reagents, such as organotin compounds and halogenated solvents, should likewise be avoided in industrial applications, and there are increasingly encouraging results in this direction with non-halogenated solvents for processing. The final challenge is to design polymers with improved stability (both thermal and photochemical) to give devices with useful operating lifetimes that can compete with inorganic modules.

Acknowledgements

This work was supported by the National Science Foundation [DMR-1407815, CHEM-1506209]. We thank Jonathan Onorato and Wesley Tatum for proof-reading the manuscript.

References

[1] Shrotriya V. Organic photovoltaics: polymer power. Nat Photonics 2009;3:447–9.
[2] Chen CC, Dou L, Zhu R, Chung CH, Song TB, Zheng YB, et al. Visibly transparent polymer solar cells produced by solution processing. ACS Nano 2012;6:7185–90.
[3] Colsmann A, Puetz A, Bauer A, Hanisch J, Ahlswede E, Lemmer U. Efficient semi-transparent organic solar cells with good transparency color perception and rendering properties. Adv Energy Mater 2011;1:599–603.
[4] Scharber MC, Mühlbacher D, Koppe M, Denk P, Waldauf C, Heeger AJ, et al. Design rules for donors in bulk-heterojunction solar cells—towards 10% energy-conversion efficiency. Adv Mater 2006;18:789–94.
[5] Brabec CJ. Organic photovoltaics: technology and market. Sol Energy Mater Sol Cells 2004;83:273–92.
[6] Wienk MM, Kroon JM, Verhees WJH, Knol J, Hummelen JC, van Hal PA, et al. Efficient methano[70] fullerene/MDMO-PPV bulk heterojunction photovoltaic cells. Angew Chem Int Ed 2003;42:3371–5.
[7] Dang MT, Hirsch L, Wantz G. P3HT:PCBM, best seller in polymer photovoltaic research. Adv Mater 2011;23:3597–602.
[8] Liu CC, Wang K, Gong X, Heeger AJ. Low bandgap semiconducting polymers for polymeric photovoltaics. Chem Soc Rev 2016;45:4825–46.
[9] Son HJ, He F, Carsten B, Yu L. Are we there yet? Design of better conjugated polymers for polymer solar cells. J Mater Chem 2011;21:18934–45.
[10] Guo X, Baumgarten M, Müllen K. Designing Π-conjugated polymers for organic electronics. Prog Polym Sci 2013;38:1832–908.
[11] Nielsen CB, Holliday S, Chen HY, Cryer SJ, McCulloch I. Non-fullerene electron acceptors for use in organic solar cells. Acc Chem Res 2015;48:2803–12.
[12] Lin Y, Zhan X. Non-fullerene acceptors for organic photovoltaics: an emerging horizon. Mater Hori 2014;1:470–88.

[13] Cao W, Xue J. Recent progress in organic photovoltaics: device architecture and optical design. Energy Environ Sci 2014;7:2123–44.
[14] Chen LM, Xu Z, Hong Z, Yang Y. Interface investigation and engineering – achieving high performance polymer photovoltaic devices. J Mater Chem 2010;20:2575–98.
[15] Gregg BA, Hanna MC. Comparing organic to inorganic photovoltaic cells: theory, experiment, and simulation. J Appl Phys 2003;93:3605–14.
[16] Tang CW. Two-layer organic photovoltaic cell. Appl Phys Lett 1986;48:183–5.
[17] Proctor CM, Kuik M, Nguyen TQ. Charge carrier recombination in organic solar cells. Prog Polym Sci 2013;38:1941–60.
[18] Hiramoto M, Fujiwara H, Yokoyama M. Three-layered organic solar cell with a photoactive interlayer of codeposited pigments. Appl Phys Lett 1991;58:1062–4.
[19] Sariciftci NS, Smilowitz L, Heeger AJ, Wudl F. Semiconducting polymers (as donors) and buckminsterfullerene (as acceptor): photoinduced electron transfer and heterojunction devices. Synth Met 1993;59:333–52.
[20] Elumalai NK, Uddin A. Open circuit voltage of organic solar cells: an in-depth review. Energy Environ Sci 2016;9:391–410.
[21] Qi B, Wang J. Fill factor in organic solar cells. Phys Chem Chem Phys 2013;15:8972–82.
[22] Madogni VI, Kounouhéwa B, Akpo A, Agbomahéna M, Hounkpatin SA, Awanou CN. Comparison of degradation mechanisms in organic photovoltaic devices upon exposure to a temperate and a subequatorial climate. Chem Phys Lett 2015;640:201–14.
[23] Wang M, Hill IG. Fluorinated alkyl phosphonic acid SAMs replace PEDOT:PSS in polymer semiconductor devices. Org Electron 2012;13:498–505.
[24] Nam S, Seo J, Woo S, Kim WH, Kim H, Bradley DDC, et al. Inverted polymer fullerene solar cells exceeding 10% efficiency with poly(2-ethyl-2-oxazoline) nanodots on electron-collecting buffer layers. Nat Commun 2015;6(8929):1–9.
[25] He Z, Zhong C, Su S, Xu M, Wu H, Cao Y. Enhanced power-conversion efficiency in polymer solar cells using an inverted device structure. Nat Photonics 2012;6:591–5.
[26] Hummelen JC, Knight BW, LePeq F, Wudl F, Yao J, Wilkins CL. Preparation and characterization of fulleroid and methanofullerene derivatives. J Org Chem 1995;60:532–8.
[27] Schroeder BC, Li Z, Brady MA, Faria GC, Ashraf RS, Takacs CJ, et al. Enhancing fullerene-based solar cell lifetimes by addition of a fullerene dumbbell. Angew Chem Int Ed 2014;53:12870–5.
[28] Holliday S, Ashraf RS, Nielsen CB, Kirkus M, Röhr JA, Tan CH, et al. A rhodanine flanked nonfullerene acceptor for solution-processed organic photovoltaics. J Am Chem Soc 2015;137:898–904.
[29] Rondeau-Gagné S, Curutchet C, Grenier F, Scholes GD, Morin JF. Synthesis, characterization and DFT calculations of new ethynyl-bridged C60 derivatives. Tetrahedron 2010;66:4230–42.
[30] Gong X, Tong M, Brunetti FG, Seo J, Sun Y, Moses D, et al. Bulk heterojunction solar cells with large open-circuit voltage: electron transfer with small donor-acceptor energy offset. Adv Mater 2011;23:2272–7.
[31] Facchetti A. Polymer donor–polymer acceptor (all-polymer) solar cells. Mater Today 2013;16:123–32.
[32] Eftaiha AF, Sun J, Hill IG, Welch GC. Recent advances of non-fullerene, small molecular acceptors for solution processed bulk heterojunction solar cells. J Mater Chem A 2014;2:1201–13.
[33] Zhao W, Qian D, Zhang S, Li S, Inganäs O, Gao F, et al. Fullerene-free polymer solar cells with over 11% efficiency and excellent thermal stability. Adv Mater 2016;28:4734–9.
[34] Kim Y, Song CE, Moon SJ, Lim E. Rhodanine dye-based small molecule acceptors for organic photovoltaic cells. Chem Commun 2014;50:8235–8.
[35] Shi H, Fu W, Shi M, Ling J, Chen H. A solution-processable bipolar diketopyrrolopyrrole molecule used as both electron donor and acceptor for efficient organic. J Mater Chem A 2015;3:1902–5.
[36] Hartnett PE, Timalsina A, Matte HSSR, Zhou N, Guo X, Zhao W, et al. Slip-stacked perylenediimides as an alternative strategy for high efficiency nonfullerene acceptors in organic photovoltaics. J Am Chem Soc 2014;136:16345–56.
[37] Chen HY, Golder J, Yeh SC, Lin CW, Chen CT, Chen CT. Diindeno[1, 2-g:1', 2'-s]rubicene: all-carbon non-fullerene electron acceptor for efficient bulk-heterojunction organic solar cells with high open-circuit voltage. RSC Adv 2015;5:3381–5.
[38] Cnops K, Zango G, Genoe J, Heremans P, Martinez-Diaz MV, Torres T, et al. Energy level tuning of non-fullerene acceptors in organic solar cells. J Am Chem Soc 2015;137:8991–7.
[39] Holliday S, Ashraf RS, Wadsworth A, Baran D, Yousaf SA, Nielsen CB, et al. High-efficiency and air-stable P3HT-based polymer solar cells with a new non-fullerene acceptor. Nat Commun 2016;7(11585):1–11.
[40] Bin H, Zhang ZG, Gao L, Chen S, Zhong L, Xue L, et al. Non-fullerene polymer solar cells based on alkylthio and fluorine substituted 2D-conjugated polymers reach 9.5% efficiency. J Am Chem Soc 2016;138:4657–64.
[41] Zhao J, Li Y, Lin H, Liu Y, Jiang K, Mu C, et al. High-efficiency non-fullerene organic solar cells enabled by a difluorobenzothiadiazole-based donor polymer combined with a properly matched small molecule acceptor. Energy Environ Sci 2015;8:520–5.
[42] Cheng P, Zhao X, Zhou W, Hou J, Li Y, Zhan X. Towards high-efficiency non-fullerene organic solar cells: matching small molecule/polymer donor/acceptor. Org Electron 2014;15:2270–6.
[43] Brabec CJ, Heeney M, McCulloch I, Nelson J. Influence of blend microstructure on bulk heterojunction organic photovoltaic performance. Chem Soc Rev 2011;40:1185–99.
[44] Liu F, Gu Y, Shen X, Ferdous S, Wang HW, Russell TP. Characterization of the morphology of solution-processed bulk heterojunction organic photovoltaics. Prog Polym Sci 2013;38:1990–2052.
[45] Huang Y, Kramer EJ, Heeger AJ, Bazan GC. Bulk heterojunction solar cells: morphology and performance relationships. Chem Rev 2014;114:7006–43.
[46] Vakhshouri K, Kesava SV, Kozub DR, Gomez ED. Characterization of the mesoscopic structure in the photoactive layer of organic solar cells: a focused review. Mater Lett 2013;90:97–102.
[47] Rajaram S, Shivanna R, Kandappa SK, Narayan KS. Nonplanar perylene diimides as potential alternatives to fullerenes in organic solar cells. J Phys Chem Lett 2012;3:2405–8.
[48] Park JH, Kim JS, Lee JH, Lee WH, Cho K. Effect of annealing solvent solubility on the performance of poly(3-hexylthiophene)/methanofullerene solar cells. J Phys Chem C 2009;113:17579–84.
[49] Treat ND, Brady MA, Smith G, Toney MF, Kramer EJ, Hawker CJ, et al. Interdiffusion of PCBM and P3HT reveals miscibility in a photovoltaically active blend. Adv Energy Mater 2011;1:82–9.
[50] Collins BA, Gann E, Guignard L, He X, McNeill CR, Ade H. Molecular miscibility of polymer-fullerene blends. J Phys Chem Lett 2010;1:3160–6.
[51] Razzell-Hollis J, Limbu S, Kim JS. Spectroscopic investigations of three-phase morphology evolution in polymer: fullerene solar cell blends. J Phys Chem C 2016;120:10806–14.
[52] Collins BA, Li Z, Tumbleston JR, Gann E, McNeill CR, Ade H. Absolute measurement of domain composition and nanoscale size distribution explains performance in PTB7:PC71BM solar cells. Adv Energy Mater 2013;3:65–74.
[53] Yan H, Collins BA, Gann E, Wang C, Ade H, McNeill CR. Correlating the efficiency and nanomorphology of polymer blend solar cells utilizing resonant soft X-ray scattering. ACS Nano 2012;6:677–88.
[54] Chen W, Xu T, He F, Wang W, Wang C, Strzalka J, et al. Hierarchical nanomorphologies promote exciton dissociation in polymer/fullerene bulk heterojunction solar cells. Nano Lett 2011;11:3707–13.
[55] Liu F, Zhao W, Tumbleston JR, Wang C, Gu Y, Wang D, et al. Understanding the morphology of PTB7:PCBM blends in organic photovoltaics. Adv Energy Mater 2014;4(1301377):1–9.
[56] Leman D, Kelly MA, Ness S, Engmann S, Herzing A, Snyder C, et al. In situ characterization of polymer–fullerene bilayer stability. Macromolecules 2015;48:383–92.
[57] Shoaee S, Subramaniyan S, Xin H, Keiderling C, Tuladhar PS, Jamieson F, et al. Charge photogeneration for a series of thiazolo-thiazole donor polymers blended with the fullerene electron acceptors PCBM and ICBA. Adv Funct Mater 2013;23:3286–98.
[58] Burke TM, McGehee MD. How high local charge carrier mobility and an energy cascade in a three-phase bulk heterojunction enable >90% quantum efficiency. Adv Mater 2014;26:1923–8.
[59] Foster S, Deledalle F, Mitani A, Kimura T, Kim KB, Okachi T, et al. Electron collection as a limit to polymer:PCBM solar cell efficiency: effect of blend microstructure on carrier mobility and device performance in PTB7:PCBM. Adv Energy Mater 2014;4(1400311):1–12.
[60] Albrecht S, Tumbleston JR, Janietz S, Dumsch I, Allard S, Scherf U, et al. Quantifying charge extraction in organic solar cells: the case of fluorinated PCPDTBT. J Phys Chem Lett 2014;5:1131–8.
[61] Hedley GJ, Ward AJ, Alekseev A, Howells CT, Martins ER, Serrano LA, et al. Determining the optimum morphology in high-performance polymer-fullerene organic photovoltaic cells. Nat Commun 2013;4(2867):1–10.
[62] Liu Y, Zhao J, Li Z, Mu C, Ma W, Hu H, et al. Aggregation and morphology control enables multiple cases of high-efficiency polymer solar cells. Nat Commun 2014;5(5293):1–8.
[63] Ro HW, Downing JM, Engmann S, Herzing AA, DeLongchamp DM, Richter LJ, et al. Morphology changes upon scaling a high-efficiency, solution-processed solar cell. Energy Environ Sci 2016;9:2835–46.
[64] Tumbleston JR, Stuart AC, Gann E, You W, Ade H. Fluorinated polymer yields high organic solar cell performance for a wide range of morphologies. Adv Funct Mater 2013;23:3463–70.
[65] Na JY, Kang B, Sin DH, Cho K, Park YD. Understanding solidification of polythiophene thin films during spin-coating: effects of spin-coating time and processing additives. Sci Rep 2015;5(13288):1–14.
[66] Chou KW, Yan B, Li R, Li EQ, Zhao K, Anjum DH, et al. Spin-cast bulk heterojunction solar cells: a dynamical investigation. Adv Mater 2013;25:1923–9.
[67] Teichler A, Perelaer J, Schubert US. Inkjet printing of organic electronics – comparison of deposition techniques and state-of-the-art developments. J Mater Chem C 2013;1:1910–25.
[68] Liao HC, Ho CC, Chang CY, Jao MH, Darling SB, Su WF. Additives for morphology control in high-efficiency organic solar cells. Mater Today 2013;16:326–36.
[69] Hammond MR, Kline RJ, Herzing AA, Richter LJ, Germack DS, Ro H, et al. Molecular order in high-efficiency polymer/fullerene bulk heterojunction solar cells. ACS Nano 2011;5:8248–57.
[70] Bartelt JA, Douglas JD, Mateker WR, El Labban A, Tassone CJ, Toney MF, et al. Controlling solution-phase polymer aggregation with molecular weight and

solvent additives to optimize polymer-fullerene bulk heterojunction solar cells. Adv Energy Mater 2014;4(1301733):1–11.
[71] Lou SJ, Szarko JM, Xu T, Yu L, Marks TJ, Chen LX. Effects of additives on the morphology of solution phase aggregates formed by active layer components of high-efficiency organic solar cells. J Am Chem Soc 2011;133:20661–3.
[72] Kniepert J, Lange I, Heidbrink J, Kurpiers J, Brenner TJK, Koster LJA, et al. Effect of solvent additive on generation, recombination, and extraction in PTB7:PCBM solar cells: a conclusive experimental and numerical simulation study. J Phys Chem C 2015;119:8310–20.
[73] Li N, Brabec CJ. Air-processed polymer tandem solar cells with power conversion efficiency exceeding 10%. Energy Environ Sci 2015;8:2902–9.
[74] Tournebize A, Rivaton A, Peisert H, Chassé T. The crucial role of confined residual additives on the photostability of P3HT:PCBM active layers. J Phys Chem C 2015;119:9142–8.
[75] de Villers BJT, O'Hara KA, Ostrowski DP, Biddle PH, Shaheen SE, Chabinyc ML, et al. Removal of residual diiodooctane improves photostability of high-performance organic solar cell polymers. Chem Mater 2016;28:876–84.
[76] Sista P, Luscombe CK. Progress in the synthesis of poly (3-hexylthiophene. Adv Polym Sci 2014;265:1–38.
[77] Holliday S, Donaghey JE, McCulloch I. Advances in charge carrier mobilities of semiconducting polymers used in organic transistors. Chem Mater 2014;26:647–63.
[78] Nielsen CB, McCulloch I. Recent advances in transistor performance of polythiophenes. Prog Polym Sci 2013;38:2053–69.
[79] McCulloch I, Ashraf RS, Biniek L, Bronstein H, Combe C, Donaghey JE, et al. Design of semiconducting indacenodithiophene polymers for high performance transistors and solar cells. Acc Chem Res 2012;45:714–22.
[80] Bundgaard E, Krebs FC. Low band gap polymers for organic photovoltaics. Sol Energy Mater Sol Cells 2007;91:954–85.
[81] Müllen K, Pisula W. Donor–acceptor polymers. (Editorial). J Am Chem Soc 2015;137:9503–5.
[82] Meyer F. Fluorinated conjugated polymers in organic bulk heterojunction photovoltaic solar cells. Prog Polym Sci 2015;47:70–91.
[83] Lu L, Zheng T, Wu Q, Schneider AM, Zhao D, Yu L. Recent advances in bulk heterojunction polymer. Solar Cells 2015;115:12666–731.
[84] Lu L, Yu L. Understanding low bandgap polymer PTB7 and optimizing polymer solar cells based on it. Adv Mater 2014;26:4413–30.
[85] Yao H, Ye L, Zhang H, Li S, Zhang S, Hou J. Molecular design of benzodithiophene-based organic photovoltaic materials. Chem Rev 2016;116:7397–457.
[86] Zhang S, Ye L, Hou J. Breaking the 10% efficiency barrier in organic photovoltaics: morphology and device optimization of well-Known PBDTTT polymers. Adv Energy Mater 2016;6(1502529):1–20.
[87] Neef CJ, Brotherston ID, Ferraris JP. Synthesis and electronic properties of poly(2-phenylthieno[3,4-b]thiophene): a new low band gap polymer. Chem Mater 1999;11:1957–8.
[88] Lee K, Sotzing G. Poly(thieno[3,4-b]thiophene): a new stable low band gap conducting polymer. Macromolecules 2001;34:5746–7.
[89] Sotzing G, Lee K. Poly(thieno[3,4-b]thiophene): a p- and n-dopable polythiophene exhibiting high optical transparency in the semiconducting state. Macromolecules 2002;35:7281–6.
[90] Pomerantz M, Gu X. Poly(2-decylthieno[3,4-b]thiophene): a new soluble low-bandgap conducting polymer. Synth Met 1997;84:243–4.
[91] Liang Y, Wu Y, Feng D, Tsai ST, Son HJ, Li G, et al. Development of new semiconducting polymers for high performance solar cells. J Am Chem Soc 2009;131:56–7.
[92] Guo J, Liang Y, Szarko J, Lee B, Son HJ, Rolczynski BS, et al. Structure, dynamics, and power conversion efficiency correlations in a new low bandgap polymer: PCBM solar cell. J Phys Chem B 2010;114:742–8.
[93] Liang Y, Feng D, Wu Y, Tsai ST, Li G, Ray C, et al. Highly efficient solar cell polymers developed via fine-tuning of structural and electronic properties. J Am Chem Soc 2009;131:7792–9.
[94] Liang Y, Xu Z, Xia J, Tsai ST, Wu Y, Li G, et al. For the bright future—bulk heterojunction polymer solar cells with power conversion efficiency of 7.4%. Adv Mater 2010;22:E135–8.
[95] Ouyang X, Peng R, Ai L, Zhang X, Ge Z. Efficient polymer solar cells employing a non-conjugated small-molecule electrolyte. Nat Photonics 2015;9:520–4.
[96] Lin Y, Zhao F, He Q, Huo L, Wu Y, Parker TC, et al. High-performance electron acceptor with thienyl side chains for organic photovoltaics. J Am Chem Soc 2016;138:4955–61.
[97] Huang J, Carpenter JH, Li CZ, Yu JS, Ade H, Jen AKY. Highly efficient organic solar cells with improved vertical donor–acceptor compositional gradient via an inverted off-center spinning method. Adv Mater 2016;28:967–74.
[98] Adhikary P, Venkatesan S, Adhikari N, Maharjan PP, Adebanjo O, Chen J, et al. Enhanced charge transport and photovoltaic performance of PBDTTT-C-T/PC70BM solar cells via UV-ozone treatment. Nanoscale 2013;5:10007–13.
[99] Guo X, Zhang M, Ma W, Ye L, Zhang S, Liu S, et al. Enhanced photovoltaic performance by modulating surface composition in bulk heterojunction polymer solar cells based on PBDTTT-C-T/PC71BM. Adv Mater 2014;26:4043–9.
[100] Liu P, Zhang K, Liu F, Jin Y, Liu S, Russell TP, et al. Effect of fluorine content in thienothiophene-benzodithiophene copolymers on the morphology and performance of polymer solar cells. Chem Mater 2014;26:3009–17.
[101] Zhang M, Guo X, Zhang S, Hou J. Synergistic effect of fluorination on molecular energy level modulation in highly efficient photovoltaic polymers. Adv Mater 2014;26:1118–23.
[102] Dou L, Chang WH, Gao J, Chen CC, You J, Yang Y. A selenium-substituted low-bandgap polymer with versatile photovoltaic applications. Adv Mater 2013;25:825–31.
[103] Saadeh HA, Lu L, He F, Bullock JE, Wang W, Carsten B, et al. Polyselenopheno[3,4-b]selenophene for highly efficient bulk heterojunction solar cells. ACS Macro Lett 2012;1:361–5.
[104] Chang WH, Meng L, Dou L, You J, Chen CC, Yang Y, et al. A selenophene containing benzodithiophene-alt-thienothiophene polymer for additive-Free high performance solar cell. Macromolecules 2015;48:562–8.
[105] Zhang S, Ye L, Zhao W, Liu D, Yao H, Hou J. Side chain selection for designing highly efficient photovoltaic polymers with 2D-conjugated structure. Macromolecules 2014;47:4653–9.
[106] Cheng YJ, Luo J, Huang S, Zhou X, Shi Z, Kim TD, et al. Donor-acceptor thiolated polyenic chromophores exhibiting large optical nonlinearity and excellent photostability. Chem Mater 2008;20:5047–54.
[107] Cui C, Wong WY, Li Y. Improvement of open-circuit voltage and photovoltaic properties of 2D-conjugated polymers by alkylthio substitution. Energy Environ Sci 2014;7:2276–84.
[108] Ye L, Zhang S, Zhao W, Yao H, Hou J. Highly efficient 2D-conjugated benzodithiophene-based photovoltaic polymer with linear alkylthio side chain. Chem Mater 2014;26:3603–5.
[109] Zhang S, Uddin MA, Zhao W, Ye L, Woo HY, Liu D, et al. Optimization of side chains in alkylthiothiophene-substituted benzo[1, 2-b:4, 5-b']dithiophene-based photovoltaic polymers. Polym Chem 2015;6:2752–60.
[110] Yao H, Zhao W, Zheng Z, Cui Y, Zhang J, Wei Z, et al. PBDT-TSR: a highly efficient conjugated polymer for polymer solar cells with a regioregular structure. J Mater Chem A 2016;4:1708–13.
[111] Liu J, Li X, Zhang S, Ren X, Cheng J, Zhu L, et al. Synergic effects of randomly aligned SWCNT mesh and self-assembled molecule layer for high-performance, low-bandgap, polymer solar cells with fast charge extraction. Adv Mater Interfaces 2015;2(1500324):1–9.
[112] Cui C, He Z, Wu Y, Cheng X, Wu H, Li Y, et al. High-performance polymer solar cells based on a 2D-conjugated polymer with an alkylthio side-chain. Energy Environ Sci 2016;9:885–91.
[113] Qian D, Ye L, Zhang M, Liang Y, Li L, Huang Y, et al. Design, application, and morphology study of a new photovoltaic polymer with strong aggregation in solution state. Macromolecules 2012;45:9611–7.
[114] Tan Z, Li S, Wang F, Qian D, Lin J, Hou J, et al. High performance polymer solar cells with as-prepared zirconium acetylacetonate film as cathode buffer layer. Sci Rep 2014;4(4691):1–9.
[115] Graham KR, Cabanetos C, Jahnke JP, Idso MN, El Labban A, Ndjawa GON, et al. Importance of the Donor:Fullerene intermolecular arrangement for high-efficiency organic photovoltaics. J Am Chem Soc 2014;136:9608–18.
[116] Huo L, Liu T, Fan B, Zhao Z, Sun X, Wei D. Organic solar cells based on a 2D benzo [1,2-b:4,5-b′]difuran-conjugated polymer with high-power conversion effi ciency. Adv Mater 2015;27:6969–75.
[117] Liu T, Meng D, Cai Y, Sun X, Li Y, Huo L, et al. High-performance non-fullerene organic solar cells based on a selenium-containing polymer donor and a twisted perylene bisimide acceptor. Adv Sci 2016;3(1600117):1–6.
[118] Huo L, Liu T, Sun X, Cai Y, Heeger AJ, Sun Y. Single-Junction organic solar cells based on a novel wide-bandgap polymer with efficiency of 9.7%. Adv Mater 2015;27:2938–44.
[119] Casey A, Ashraf RS, Fei Z, Heeney M. Thioalkyl-substituted benzothiadiazole acceptors: copolymerization with carbazole affords polymers with large stokes shifts and high solar cell voltages. Macromolecules 2014;47:2279–88.
[120] Casey A, Dimitrov SD, Shakya-Tuladhar P, Fei Z, Nguyen M, Han Y, et al. Effect of systematically tuning conjugated donor polymer lowest unoccupied molecular orbital levels via cyano substitution on organic photovoltaic device performance. Chem Mater 2016;28:5110–20.
[121] Neto BAD, Lapis AAM, da Silva Júnior EN, Dupont J. 2,1,3-Benzothiadiazole and derivatives: synthesis, properties, reactions, and applications in light technology of small molecules. Eur J Org Chem 2013;2013:228–55.
[122] Gao M, Subbiah J, Geraghty PB, Chen M, Purushothaman B, Chen X, et al. Development of a high-performance donor–acceptor conjugated polymer: synergy in materials and device optimization. Chem Mater 2016;28:3481–7.
[123] Zhang M, Gu Y, Guo X, Liu F, Zhang S, Huo L, et al. Efficient polymer solar cells based on benzothiadiazole and alkylphenyl substituted benzodithiophene with a power conversion efficiency over 8%. Adv Mater 2013;25:4944–9.
[124] Lan L, Chen Z, Hu Q, Ying L, Zhu R, Liu F, et al. High-performance polymer solar cells based on a wide- bandgap polymer containing pyrrolo [3, 4-f] benzotriazole-5, 7-dione with a power conversion efficiency of 8.63%. Adv Sci 2016;3(1600032):1–7.
[125] Cabanetos C, El Labban A, Bartelt JA, Douglas JD, Mateker WR, Fréchet JMJ, et al. Linear side chains in benzo[1,2-b:4,5-bé]dithiophene–thieno[3,4-c]pyrrole-4,6-dione polymers direct self-assembly and solar cell performance. J Am Chem Soc 2013;135:4656–9.
[126] Piliego C, Holcombe TW, Douglas JD, Woo CH, Beaujuge PM, Fréchet JMJ. Synthetic control of structural order in N-Alkylthieno[3,4-c]pyrrole-4,6-dione-based polymers for efficient solar cells. J Am Chem Soc 2010;132:7595–7.

[127] Zou Y, Najari A, Berrouard P, Beaupré S, Aïch BR, Tao Y, et al. A thieno[3,4-c]pyrrole-4,6-dione-based copolymer for efficient solar cells. J Am Chem Soc 2010;132:5330–1.
[128] Chen HC, Chen YH, Liu CC, Chien YC, Chou SW, Chou PT. Prominent short-circuit currents of fluorinated quinoxaline-based copolymer solar cells with a power conversion efficiency of 8.0%. Chem Mater 2012;24:4766–72.
[129] Yuan J, Qiu L, Zhang Z, Li Y, He Y, Jiang L, et al. A simple strategy to the side chain functionalization on the quinoxaline unit for efficient polymer solar cells. Chem Commun 2016;52:6881–4.
[130] Nguyen TL, Choi H, Ko SJ, Uddin MA, Walker B, Yum S, et al. Semi-crystalline photovoltaic polymers with efficiency exceeding 9% in a 300 nm thick conventional single-cell device. Energy Environ Sci 2014;7:3040–51.
[131] Li G, Kang C, Gong X, Zhang J, Li W, Li C, et al. 5,6-Difluorobenzothiadiazole and silafluorene based conjugated polymers for organic photovoltaic cells. J Mater Chem C 2014;2:5116–23.
[132] Wang N, Chen Z, Wei W, Jiang Z. Fluorinated benzothiadiazole-based conjugated polymers for high-performance polymer solar cells without any processing additives or post-treatments. J Am Chem Soc 2013;135:17060–8.
[133] Chen Z, Cai P, Chen J, Liu X, Zhang L, Lan L, et al. Low band-gap conjugated polymers with strong interchain aggregation and very high hole mobility towards highly efficient thick-film polymer solar cells. Adv Mater 2014;26:2586–91.
[134] Osaka I, Shimawaki M, Mori H, Doi I, Miyazaki E, Koganezawa T, et al. Synthesis, characterization, and transistor and solar cell applications of a naphthobisthiadiazole-based semiconducting polymer. J Am Chem Soc 2012;134:3498–507.
[135] Wang Y, Xin X, Lu Y, Xiao T, Xu X, Zhao N, et al. Substituent effects on physical and photovoltaic properties of 5,6-difluorobenzo[c][1,2,5]thiadiazole-based D–a polymers: toward a donor design for high performance polymer solar cells. Macromolecules 2013;46:9587–92.
[136] Ma W, Tumbleston JR, Wang M, Gann E, Huang F, Ade H. Domain purity, miscibility, and molecular orientation at donor/acceptor interfaces in high performance organic solar cells: paths to further improvement. Adv Energy Mater 2013;3:864–72.
[137] Stuart AC, Tumbleston JR, Zhou H, Li W, Liu S, Ade H, et al. Fluorine substituents reduce charge recombination and drive structure and morphology development in polymer solar cells. J Am Chem Soc 2013;135:1806–15.
[138] Mei J, Bao Z. Side chain engineering in solution-processable conjugated polymers. Chem Mater 2014;26:604–15.
[139] Meager I, Ashraf RS, Mollinger S, Schroeder BC, Bronstein H, Beatrup D, et al. Photocurrent enhancement from diketopyrrolopyrrole polymer solar cells through alkyl-chain branching point manipulation. J Am Chem Soc 2013;135:11537–40.
[140] Yiu AT, Beaujuge PM, Lee OP, Woo CH, Toney MF, Fréchet JMJ. Side-chain tunability of furan-containing low-band-gap polymers provides control of structural order in efficient solar cells. J Am Chem Soc 2012;134:2180–5.
[141] Chen Z, Brown J, Drees M, Seger M, Hu Y, Xia Y, et al. Benzo[d][1,2,3]thiadiazole (isoBT): synthesis, structural analysis, and implementation in semiconducting polymers. Chem Mater 2016;28:6390–400.
[142] Yao Y, Dong H, Hu W. Ordering of conjugated polymer molecules: recent advances and perspectives. Polym Chem 2013;4:5197–205.
[143] Tumbleston JR, Collins BA, Yang L, Stuart AC, Gann E, Ma W, et al. The influence of molecular orientation on organic bulk heterojunction solar cells. Nat Photonics 2014;8:385–91.
[144] Shimata Y, Ide M, Tashiro M, Katouda M, Imamura Y, Saeki A. Charge dynamics at heterojunction between face-on/edge-on PCPDTBT and PCBM bilayer: interplay of donor/acceptor distance and local charge carrier mobility. J Phys Chem C 2016;120:17887–97.
[145] Zhao J, Li Y, Yang G, Jiang K, Lin H, Ade H, et al. Efficient organic solar cells processed from hydrocarbon solvents. Nat Energy 2016;1(15027):1–7.
[146] Zhao J, Li Y, Hunt A, Zhang J, Yao H, Li Z, et al. A difluorobenzoxadiazole building block for efficient polymer solar cells. Adv Mater 2016;28:1868–73.
[147] Blouin N, Michaud A, Gendron D, Wakim S, Blair E, Neagu-Plesu R, et al. Toward a rational design of poly(2,7-Carbazole) derivatives for solar cells. J Am Chem Soc 2008;130:732–42.
[148] Fan Q, Xiao M, Liu Y, Su W, Gao H, Tan H, et al. Improved photovoltaic performance of 2D-conjugated benzodithiophene-based polymer by the side chain engineering at quinoxaline. Polym Chem 2015;6:4290–8.
[149] Zhang S, Qin Y, Uddin MA, Jang B, Zhao W, Liu D, et al. A fluorinated polythiophene derivative with stabilized backbone conformation for highly efficient fullerene and non-Fullerene polymer solar cells. Macromolecules 2016;49:2993–3000.
[150] Liu Y, Zhao W, Wu Y, Zhang J, Li G, Li W, et al. Enhancing the power conversion efficiency of polymer solar cells to 9.26% by a synergistic effect of fluoro and carboxylate substitution. J Mater Chem A 2016;4:8097–104.
[151] Liu J, Chen S, Qian D, Gautam B, Yang G, Zhao J, et al. Fast charge separation in a non-fullerene organic solar cell with a small driving force. Nat Energy 2016;1(16089):1–7.
[152] Ma T, Jiang K, Chen S, Hu H, Lin H, Li Z. Efficient low-bandgap polymer solar cells with high open-circuit voltage and good stability. Adv Energy Mater 2015;5(1501282):1–6.
[153] Fan Q, Su W, Guo X, Guo B, Li W, Zhang Y, et al. A new polythiophene derivative for high efficiency polymer solar cells with PCE over 9%. Adv Energy Mater 2016;6(1600430):1–7.
[154] Hu H, Jiang K, Yang G, Liu J, Li Z, Lin H, et al. Terthiophene-based D–A polymer with an asymmetric arrangement of alkyl chains that enables efficient polymer solar cells. J Am Chem Soc 2015;137:14149–57.
[155] Ashraf RS, Meager I, Nikolka M, Kirkus M, Planells M, Schroeder BC, et al. Chalcogenophene comonomer comparison in small band gap diketopyrrolopyrrole-based conjugated polymers for high-performing field-effect transistors and organic solar cells. J Am Chem Soc 2015;137:1314–21.
[156] Cao J, Liao Q, Du X, Chen J, Xiao Z, Zuo Q, et al. A pentacyclic aromatic lactam building block for efficient polymer solar cells. Energy Environ Sci 2013;6:3224–8.
[157] Li H, Cao J, Zhou Q, Ding L, Wang J. High-performance inverted PThTPTI:PC71BM solar cells. Nano Energy 2015;15:125–34.
[158] Li H, Earmme T, Ren G, Saeki A, Yoshikawa S, Murari NM, et al. Beyond fullerenes: design of nonfullerene acceptors for efficient organic photovoltaics. J Am Chem Soc 2014;136:14589–97.
[159] Subramaniyan S, Xin H, Kim FS, Shoaee S, Durrant JR, Jenekhe SA. Effects of side chains on thiazolothiazole-based copolymer semiconductors for high performance solar cells. Adv Energy Mater 2011;1:854–60.
[160] Hwang YJ, Li H, Courtright BAE, Subramaniyan S, Jenekhe SA. Nonfullerene polymer solar cells with 8.5% efficiency enabled by a new highly twisted electron acceptor dimer. Adv Mater 2016;28:124–31.
[161] Wang M, Cai D, Yin Z, Chen S, Du C. Asymmetric-indenothiophene-based copolymers for bulk heterojunction solar cells with 9.14% efficiency. Adv Mater 2016;28:3359–65.
[162] Dou L, Chen CC, Yoshimura K, Ohya K, Chang WH, Gao J, et al. Synthesis of 5H-Dithieno[3,2-b:2′,3′-d]pyran as an electron-rich building block for donor-acceptor type low-bandgap polymers. Macromolecules 2013;46:3384–90.
[163] Cozzolino AF, Vargas-Baca I, Mansour S, Mahmoudkhani AH. The nature of the supramolecular association of 1,2,5-Chalcogenadiazoles. J Am Chem Soc 2005;127:3184–90.
[164] Welch GC, Ronald C, Bakus II, Teat SJ, Bazan GC. Impact of regiochemistry and isoelectronic bridgehead substitution on the molecular shape and bulk organization of narrow bandgap chromophores. J Am Chem Soc 2013;135:2298–305.
[165] Lee W, Choi H, Hwang S, Kim JY, Woo HY. Efficient conventional- and inverted-type photovoltaic cells using a planar alternating polythiophene copolymer. Chem Eur J 2012;18:2551–8.
[166] Guo X, Quinn J, Chen Z, Usta H, Zheng Y, Xia Y, et al. Dialkoxybithiazole: a new building block for head-to-head polymer semiconductors. J Am Chem Soc 2013;135:1986–96.
[167] Guo X, Kim FS, Jenekhe SA, Watson MD. Phthalimide-based polymers for high performance organic thin-film transistors. J Am Chem Soc 2009;131:7206–7.
[168] Cheng Y, Qi Y, Tang Y, Zheng C, Wan Y, Huang W, et al. Controlling intramolecular conformation through nonbonding interaction for soft-conjugated materials: molecular design and optoelectronic properties. J Phys Chem Lett 2016;7:3609–15.
[169] Lewis NS, Nocera DG. Powering the planet: chemical challenges in solar energy utilization. Proc Natl Acad Sci 2006;103:15729–35.
[170] Osedach TP, Andrew TL, Bulovic V. Effect of synthetic accessibility on the commercial viability of organic photovoltaics. Energy Environ Sci 2013;6:711–8.
[171] Kalowekamo J, Baker E. Estimating the manufacturing cost of purely organic solar cells. Sol Energy 2009;83:1224–31.
[172] Gambhir A, Sandwell P, Nelson J. The future costs of OPV–A bottom-up model of material and manufacturing costs with uncertainty analysis. Sol Energy Mater Sol Cells 2016;156:49–58.
[173] Mulligan CJ, Bilen C, Zhou X, Belcher WJ, Dastoor PC. Levelised cost of electricity for organic photovoltaics. Sol Energy Mater Sol Cells 2015;133:26–31.
[174] Mulligan CJ, Wilson M, Bryant G, Vaughan B, Zhou X, Belcher WJ, et al. A projection of commercial-scale organic photovoltaic module costs. Sol Energy Mater Sol Cells 2014;120:9–17.
[175] Machui F, Hosel M, Li N, Spyropoulos GD, Ameri T, Sondergaard RR, et al. Cost analysis of roll-to-roll fabricated ITO free single and tandem organic solar modules based on data from manufacture. Energy Environ Sci 2014;7:2792–802.
[176] Green MA, Emery K, Hishikawa Y, Warta W, Dunlop ED. Solar cell efficiency tables (version 48). Prog Photovoltaics Res Appl 2016;24:905–13.
[177] Burke DJ, Lipomi DJ. Green chemistry for organic solar cells. Energy Environ Sci 2013;6:2053–66.
[178] Zhang S, Ye L, Zhang H, Hou J. Green-solvent-processable organic solar cells. Mater Today 2016;19:533–43.
[179] Bannock JH, Xu W, Baïssas T, Heeney M, de Mello JC. Rapid flow-based synthesis of poly(3-hexylthiophene) using 2-methyltetrahydrofuran as a bio-derived reaction solvent. Eur Polym J 2016;80:240–6.
[180] Liu D, Wang Z, Zhang S, Zheng Z, Yang B, Ma W, et al. Rational selection of solvents and fine tuning of morphologies toward highly efficient polymer solar cells fabricated using green solvents. RSC Adv 2015;5:69567–72.

[181] Cai W, Liu P, Jin Y, Xue Q, Liu F, Russell TP, et al. Morphology evolution in high-performance polymer solar cells processed from nonhalogenated solvent. Adv Sci 2015;2(1500095):1–7.
[182] Zhao W, Ye L, Zhang S, Sun M, Hou J. A universal halogen-free solvent system for highly efficient polymer solar cells. J Mater Chem A 2015;3:12723–9.
[183] Sprau C, Buss F, Wagner M, Landerer D, Koppitz M, Schulz A, et al. Highly efficient polymer solar cells cast from non-halogenated xylene/anisaldehyde solution. Energy Environ Sci 2015;8:2744–52.
[184] Po R, Bianchi G, Carbonera C, Pellegrino A. All that glisters is not gold: an analysis of the synthetic complexity of efficient polymer donors for polymer solar cells. Macromolecules 2015;48:453–61.
[185] Bronstein HA, Luscombe CK. Externally initiated regioregular P3HT with controlled molecular weight and narrow polydispersity. J Am Chem Soc 2009;131:12894–5.
[186] Okamoto K, Luscombe CK. Controlled polymerizations for the synthesis of semiconducting conjugated polymers. Polym Chem 2011;2:2424–34.
[187] Suraru SL, Lee JA, Luscombe CK. C–H arylation in the synthesis of Π-conjugated polymers. ACS Macro Lett 2016;5:724–9.
[188] Okamoto K, Zhang J, Housekeeper JB, Marder SR, Luscombe CK. C–H arylation reaction: atom efficient and greener syntheses of Π-conjugated small molecules and macromolecules for organic electronic materials. Macromolecules 2013;46:8059–78.
[189] Wang XF, Wang L, Wang Z, Wang Y, Tamai N, Hong Z, et al. Natural photosynthetic carotenoids for solution-processed organic bulk-heterojunction solar cells. J Phys Chem C 2013;117:804–11.
[190] Bannock JH, Krishnadasan SH, Nightingale AM, Yau CP, Khaw K, Burkitt D, et al. Continuous synthesis of device-grade semiconducting polymers in droplet-based microreactors. Adv Funct Mater 2013;23:2123–9.
[191] Moghe D, Yu P, Kanimozhi C, Patil S, Guha S. Charge transfer complex states in diketopyrrolopyrrole polymers and fullerene blends: implications for organic solar cell efficiency. Appl Phys Lett 2011;99(233307):1–3.
[192] Bassler H, Kohler A. Charge transport in organic semiconductors. Top Curr Chem 2011;312:1–66.
[193] Zhang CZ, Shen D, Yuan Y, Song MX, Li SJ, Cao H. Syntheses of planar 1,5,2,4,6,8-dithiotetrazocine derivatives and thermodynamic study on intermolecular charge transfer for developing efficient organic solar cell. Mater Chem Phys 2016;177:463–71.
[194] Vandewal K, Tvingstedt K, Gadisa A, Inganäs O, Manca JV. On the origin of the open-circuit voltage of polymer-fullerene solar cells. Nat Mater 2009;8:904–9.
[195] Heumueller T, Mateker WR, Sachs-Quintana IT, Vandewal K, Bartelt JA, Burke TM, et al. Reducing burn-in voltage loss in polymer solar cells by increasing the polymer crystallinity. Energy Environ Sci 2014;7:2974–80.
[196] Tuladhar SM, Azzouzi M, Delval F, Yao J, Guilbert AAY, Kirchartz T, et al. Low open-Circuit voltage loss in solution-processed small-molecule organic solar cells. ACS Energy Lett 2016;1:302–8.
[197] Kirchartz T, Taretto K, Rau U. Efficiency limits of organic bulk heterojunction solar cells. J Phys Chem C 2009;113:17958–66.
[198] Giebink NC, Wiederrecht GP, Wasielewski MR, Forrest SR. Thermodynamic efficiency limit of excitonic solar cells. Phys Rev B 2011;83(195326):1–6.
[199] Veldman D, Meskers SCJ, Janssen RAJ. The energy of charge-transfer states in electron donor–acceptor blends: insight into the energy losses in organic solar cells. Adv Funct Mater 2009;19:1939–48.
[200] Koster LJA, Shaheen SE, Hummelen JC. Pathways to a new efficiency regime for organic solar cells. Adv Energy Mater 2012;2:1246–53.
[201] Gruber M, Wagner J, Klein K, Hörmann U, Opitz A, Stutzmann M, et al. Thermodynamic efficiency limit of molecular donor-acceptor solar cells and its application to diindenoperylene/C60-based planar heterojunction devices. Adv Energy Mater 2012;2:1100–8.
[202] Nelson J, Kirkpatrick J. Analysis of the photovoltaic efficiency of a molecular solar cell based on a two-level system. Appl Phys A 2004;79:15–20.
[203] Nelson J, Kirkpatrick J, Ravirajan P. Factors limiting the efficiency of molecular photovoltaic devices. Phys Rev B 2004;69(035337):1–11.
[204] Godovsky D. Modeling the ultimate efficiency of polymer solar cell using Marcus theory of electron transfer. Org Electron 2011;12:190–4.
[205] Scharber MC. On the efficiency limit of conjugated polymer:fullerene-based bulk heterojunction solar cells. Adv Mater 2016;28:1994–2001.
[206] Minnaert B, Burgelman M. Efficiency potential of organic bulk heterojunction solar cells. Prog Photovoltaics Res Appl 2007;15:741–8.
[207] Servaites JD, Ratner MA, Marks TJ. Practical efficiency limits in organic photovoltaic cells: functional dependence of fill factor and external quantum efficiency. Appl Phys Lett 2009;95(163302):1–3.